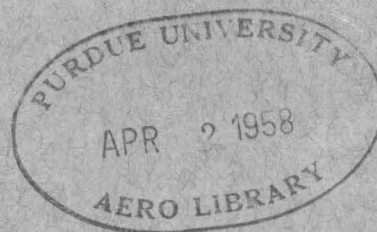


CALIFORNIA INSTITUTE OF TECHNOLOGY  
GUGGENHEIM AERONAUTICAL LABORATORY

DRANDUM No. 39

AERONAUTICAL LABORATORY

CALIFORNIA INSTITUTE OF TECHNOLOGY



## **HYPERSONIC RESEARCH PROJECT**

Memorandum No. 39

June 20, 1957

EXPERIMENTAL INVESTIGATION OF THICK,  
AXIALLY SYMMETRIC BOUNDARY LAYERS ON CYLINDERS  
AT SUBSONIC AND HYPERSONIC SPEEDS

by

Ronald L. Richmond

[ENGINEERING LIBRARY]

TECHNICAL REPORT

ARMY ORDNANCE CONTRACT NO. DA-04-495-Ord-19

GUGGENHEIM AERONAUTICAL LABORATORY  
CALIFORNIA INSTITUTE OF TECHNOLOGY  
Pasadena, California

HYPERSONIC RESEARCH PROJECT

Memorandum No. 39

June 20, 1957

EXPERIMENTAL INVESTIGATION OF THICK,  
AXIALLY SYMMETRIC BOUNDARY LAYERS ON CYLINDERS  
AT SUBSONIC AND HYPERSONIC SPEEDS

by

Ronald L. Richmond

  
Clark B. Millikan, Director  
Guggenheim Aeronautical Laboratory

ARMY ORDNANCE CONTRACT NO. DA-04-495-Ord-19  
Army Project No. 5B0306004  
Ordnance Project No. TB3-0118  
OOR Project No. 1600-PE

## ACKNOWLEDGEMENTS

The author wishes to express his sincere appreciation for the extensive advice given by Dr. Donald Coles regarding this research project and to thank William M. Sublette for his excellent help in manufacturing the experimental models. Thanks are in order also to Professor Lester Lees for his comments on this report and to Mrs. Elizabeth Fox for her unequalled typing ability displayed herein.

## ABSTRACT

An experimental investigation of the transverse curvature effect on laminar and turbulent axially symmetric boundary layers was conducted in two subsonic wind tunnels and in the GALCIT 5 x 5 inch hypersonic wind tunnel.

Subsonic turbulent skin friction coefficients were estimated from velocity profiles with axial flow on a 0.024 inch diameter cylinder and a 1.00 inch diameter cylinder. A considerable increase over the flat plate skin friction coefficient at the same momentum thickness Reynolds number was found.

Hypersonic laminar and turbulent skin friction coefficients with axial flow on an insulated 0.250 inch diameter cylinder were measured by the floating element technique and indicated, respectively, several times, and 1.5 times the laminar and turbulent flat plate skin friction coefficients at the same momentum thickness Reynolds numbers. Turbulent skin friction coefficients were estimated from pitot profiles with axial flow on a 0.064 inch diameter cylinder and on a 0.024 inch diameter cylinder at  $M_1 = 5.8$  and indicate double the value to be found for an insulated flat plate at the same momentum thickness Reynolds number.



## TABLE OF CONTENTS

PART	TITLE	PAGE
	ACKNOWLEDGEMENTS	
	ABSTRACT	
	LIST OF TABLES	
	LIST OF FIGURES	
	LIST OF SYMBOLS	
I	INTRODUCTION	1
II	THE STREAMLINE HYPOTHESIS	5
III	EXPERIMENTAL MODELS, INSTRUMENTATION, AND TECHNIQUES	10
	A. Subsonic Facilities	10
	1) Merrill Wind Tunnel	10
	2) Low Turbulence Tunnel	10
	B. Hypersonic Facility	11
IV	EXPERIMENTAL RESULTS	16
	A. Subsonic Flow	16
	1) Merrill Wind Tunnel	16
	2) Low Turbulence Tunnel	16
	B. Hypersonic Flow	17
	1) Effect of Models Extending Through the Tunnel Throat	17
	2) Alignment of the Models and Pitot Surveys	17
	3) Measured Skin Friction on the 0.250 inch Cylinder	19
V	CONCLUSIONS	20
	REFERENCES	21
	APPENDIX A: Procedure for Estimating Turbulent Skin Friction	23

## TABLE OF CONTENTS (Cont'd)

PART	TITLE	PAGE
	APPENDIX B: Computation of Displacement and Momentum Thicknesses	25
	APPENDIX C: Data Reduction Methods	27
	APPENDIX D: Reduction of Laminar Theory to Local Properties	29
	TABLES	32
	FIGURES	40

# LIST OF TABLES

TABLE NO.	TITLE	PAGE
1	Merrill Wind Tunnel Turbulent Boundary Layer Velocity Profile Data	32
2	Low Turbulence Tunnel Turbulent Boundary Layer Velocity Profile Data	33
3	Summary of Subsonic Turbulent Boundary Layer Curvature Effects	34
4	Hypersonic Boundary Layer Profile Data	35
5	Summary of Hypersonic Laminar Boundary Layer Curvature Effects	38
6	Summary of Hypersonic Turbulent Boundary Layer Curvature Effects	39

# LIST OF FIGURES

FIGURE NO.	TITLE	PAGE
1	Schematic Diagram of 1 inch Diameter Cylinder Installation in the Merrill Wind Tunnel	40
2	Schematic Diagram of 0.024 inch Wire Model Installation in the Low Turbulence Tunnel	41
3	Schematic Diagram of Cylinder Models in the 5 x 5 inch Hypersonic Tunnel (Models 1, 2, and 3)	42
4	Schematic Diagram of Cylinder Models in the 5 x 5 inch Hypersonic Tunnel (Models 4, 5, and 6)	43
5	Schematic Diagram of the 0.250 inch Skin Friction Model and Starting Shield in the 5 x 5 inch Hypersonic Tunnel	44
6	Cabinet Drawing of the 0.250 inch Skin Friction Model Floating Element Mechanism	45
7	Electric Circuit for the Skin Friction Meter	46
8	Typical Calibration of the Skin Friction Meter	47
9a, 9b	Turbulent Boundary Layer Profile with Axial Flow on a 1 inch Diameter Cylinder in the Merrill Wind Tunnel	48, 49
10a, 10b	Turbulent Boundary Layer Profile with Axial Flow on a 0.024 inch Diameter Cylinder in the Low Turbulence Tunnel	50, 51
11	Subsonic Turbulent Boundary Layer Estimated Skin Friction	52
12	Ratio of Turbulent Skin Friction on a Cylinder to that on a Flat Plate at Subsonic Speeds	53
13	Laminar Boundary Layer Profile with Axial Flow on a 0.250 inch Diameter Cylinder in the 5 x 5 inch Hypersonic Wind Tunnel	54

# LIST OF FIGURES (Cont'd)

FIGURE NO.	TITLE	PAGE
14a, 14b	Turbulent Boundary Layer Profile with Axial Flow on a 0.250 inch Diameter Cylinder in the 5 x 5 inch Hypersonic Wind Tunnel	55, 56
15	Laminar Boundary Layer Profile with Axial Flow on a 0.064 inch Diameter Cylinder in the 5 x 5 inch Hypersonic Wind Tunnel	57
16a, 16b	Turbulent Boundary Layer Profile with Axial Flow on a 0.064 inch Diameter Cylinder in the 5 x 5 inch Hypersonic Wind Tunnel	58, 59
17	Laminar Boundary Layer Profile with Axial Flow on a 0.024 inch Diameter Cylinder in the 5 x 5 inch Hypersonic Wind Tunnel	60
18a, 18b	Turbulent Boundary Layer Profile with Axial Flow on a 0.024 inch Diameter Cylinder in the 5 x 5 inch Hypersonic Wind Tunnel	61, 62
19	Computed Momentum Thickness Reynolds Number on the 0.250 inch Skin Friction Model	63
20	Measured Skin Friction on the 0.250 inch Model Versus Tunnel Reservoir Pressure	64
21	Hypersonic Laminar and Turbulent Boundary Layer Skin Friction	65
22	Ratio of Skin Friction on a Cylinder to that on a Flat Plate at $M_1 = 0$ and $M_1 = 5.8$ at constant $R_\theta$	66

# LIST OF SYMBOLS

SYMBOLS	DESCRIPTION
C	constant found in equation 3
$C_f$	local skin friction coefficient
d	circular cylinder diameter $\approx 2r_o$
f	boundary layer function found in equation 1 and reference 10
F	function found in equation 10
G	function found in equation 9
H	function found in equation 6
$l$	length of a body in x flow direction
M	Mach number
$M_1$	free stream Mach number
P	local static pressure
$P_o$	tunnel reservoir pressure
$P_o'$	local stagnation pressure behind a normal shock
q	free stream dynamic pressure $\approx \frac{1}{2}\rho_1 u_1^2$
r	radial distance from circular cylinder axis
$r_o$	circular cylinder radius
R	free stream Reynolds number
T	local static temperature (absolute)
$T_1$	free stream static temperature
$T_o$	stagnation temperature
$T_w$	wall recovery temperature
$u, U$	local axial velocity
$u_1, U_1$	free stream velocity
$u_\tau, U_\tau$	turbulent boundary layer "friction velocity"

## LIST OF SYMBOLS (Cont'd)

SYMBOL	DESCRIPTION
$v$	local radial velocity
$x$	axial dimension
$y$	radial or lateral distance from the surface of a cylinder or flat plate $= r - r_0$ for a cylinder

## GREEK SYMBOLS

$\delta$	boundary layer thickness
$\delta^*$	boundary layer displacement thickness defined in Appendix B
$\mu_1$	free stream coefficient of viscosity
$\mu_w$	wall value of viscosity coefficient
$\nu$	coefficient of kinematic viscosity $= \mu/\rho$
$\Phi$	function found in equation 3
$\Psi$	streamfunction
$\rho$	local density
$\rho_1$	free stream density
$\rho_w$	density of fluid at a wall
$\rho_\tau$	turbulent boundary layer "friction density"
$\tau_w$	wall value of shearing stress
$\theta$	boundary layer momentum thickness defined in Appendix B

# I. INTRODUCTION\*

## Laminar Incompressible Boundary Layer Theories

Seban and Bond (1) have numerically solved the non-linear laminar boundary layer equations for the region of a circular cylinder near the nose where the basic laminar flow parameter  $\nu x / u_1 r_0^2$  is small. Their solution was later pointed out to be in error and subsequently corrected by Kelly (2). An error in skin friction coefficient resulted from small numerical mistakes. Another error pointed out by Kelly was due to a physically incoherent definition of displacement thickness. For a boundary layer on a cylinder subjected to axial flow, the definition of  $\delta^*$  which physically corresponds to that on a flat plate is

$$\int_{r_0}^{\delta^* + r_0} \rho u_1^2 \pi r dr = \int_{r_0}^{\delta + r_0} \rho (u_1 - u) 2 \pi r dr$$

or

$$(\delta^* + r_0)^2 - r_0^2 = 2 \int_{r_0}^{\delta + r_0} (u_1 - u) r dr$$

This definition of  $\delta^*$  was used earlier by Moore (3).

Cooper and Tulin (4), upon linearizing the Prandtl boundary layer equations, obtained a series solution for the friction on a circular cylinder in terms of powers of  $\nu x / u_1 r_0^2$  for small values of that parameter and in terms of inverse powers of  $\ln(4\nu x / cu_1 r_0^2)$  for large values of  $\nu x / u_1 r_0^2$ . Flows with non-steady motion and pressure gradient were also treated.

For values of the parameter  $\nu x / u_1 r_0^2$  greater than 100

---

\* This investigation was carried out under the sponsorship and with the financial support of the Office, Chief of Ordnance, and the Office of Ordnance Research, U. S. Army (Contract No. DA-04-495-Ord-19).



Glauert and Lighthill (5) have obtained a series solution for the skin friction on a circular cylinder in terms of inverse powers of  $\ln(4\nu x/u_1 r_0^2)$ . In addition a Pohlhausen type solution was obtained for arbitrary  $\nu x/u_1 r_0^2$  giving, however, too low a value of skin friction. A complete curve of skin friction versus  $\nu x/u_1 r_0^2$  using the Seban-Bond-Kelly solution for  $\nu x/u_1 r_0^2$  less than 0.04, the Pohlhausen solution plus an arbitrary 9 percent for the range  $0.04 < \nu x/u_1 r_0^2 < 100$ , and the series solution for  $\nu x/u_1 r_0^2$  greater than 100 was presented.

For  $\nu x/u_1 r_0^2$  approaching infinity Stewartson (6) has also solved for the skin friction on a circular cylinder in terms of inverse powers of  $\ln(4\nu x/Cu_1 r_0^2)$  with the object of investigating laminar separation. The qualitative conclusion reached was that a thick, axially symmetric laminar boundary layer on a cylinder tends to delay separation.

Mark (7) has attempted to bridge the gap in  $\nu x/u_1 r_0^2$  between the Stewartson result and the Seban-Bond-Kelly result by using assumed velocity profiles in von Karman's momentum integral relationship. Mark's approximation gave a lower value of laminar skin friction than either of the more exact analyses.

The primary qualitative result of all the above analyses is that the skin friction coefficient for an external axially symmetric laminar boundary layer on a cylinder is greater than that on a flat plate for similar boundary layer thicknesses. Glauert and Lighthill very aptly point out that fluid acceleration in the boundary layer near the solid boundary is small. This results in the

requirement that the shear force on succeeding cylindrical fluid surfaces near the cylinder wall be the same (i.e.  $2\pi r\tau$  is approximately constant near the wall). Therefore, near the wall, the shear stress  $\tau$  and hence  $\partial u/\partial r$  vary like  $1/r$  and thus indicate a larger value of skin friction than would exist on a comparable flat plate.

#### Laminar Compressible Boundary Layer Theories

Mark (7), as in the subsonic case, has used assumed velocity profiles in von Karman's momentum integral relation to obtain  $C_f \sqrt{R_x}$  as a function of  $u_1 r_0^2/4\nu x$  with Mach number as a parameter. He shows that at  $M_1 = 5.8$  for  $u_1 r_0^2/4\nu x > 10^5$ , essentially the flat plate solution is obtained.

Probstein and Elliott (8) generalized Mangler's transformation to obtain simpler boundary layer equations in the two regions  $\delta^*/r_0 \gg 1$  and  $\delta^*/r_0 \leq 1$ . In the latter region the first order correction to Mangler's solution for a circular cylinder was obtained by numerical integration.

The above two papers show that the transverse curvature has a greater effect on laminar skin friction, the higher the Mach number. Probstein and Elliott show that the transverse curvature term in the momentum and energy equations behaves as would a favorable pressure gradient, readily explaining an increase in skin friction and heat transfer coefficient and a delay in transition and separation. This term does not, however, significantly change the temperature recovery factor.

### Turbulent Boundary Layer Theories

Eckert (9) has attempted to determine the effect of lateral curvature on turbulent skin friction when the boundary layer thickness  $\delta$  becomes as large as the cylinder radius. After many simplifying assumptions it was found that when  $\delta/r_0 = 1$ , the incompressible local turbulent skin friction coefficient is 6 percent greater than that on a flat plate at the same Reynolds number based on  $x$ . Similarly an 8.5 percent increase was found at Mach 10. He concludes that these values of skin friction are probably too low.

It is this author's opinion that the only reliable method of attack on the turbulent, axially symmetric boundary layer on a cylinder is by way of extensive experimentation, especially in view of the lack of basic knowledge of turbulent processes even on flat plates.

Recently an effort has been made by Coles (10, 11, 12, 13) to interpret various experimental investigations of turbulent boundary layer flow from the point of view of similarity laws. Of particular importance here is the "streamline hypothesis" as proposed by Coles (11).

## II. THE STREAMLINE HYPOTHESIS

For subsonic turbulent boundary layer flow on a flat plate experiments indicate the existence of a universal function

$$u/u_\tau = f(yu_\tau/\nu) \quad (1)$$

which is independent of pressure gradient. The "friction velocity",  $u_\tau$ , is defined by the expression

$$\tau_w = \rho u_\tau^2 \quad (2)$$

Coles (11) has shown that equation 1, when appropriately combined with the continuity equation, implies that  $u/u_\tau$  is constant on mean streamlines. The assumption that this latter property is generally valid is the "streamline hypothesis".

To develop an expression comparable to (1) for supersonic turbulent boundary layer flow on a cylinder we will assume the "streamline hypothesis" in the form

$$u/u_\tau = \Phi(C\Psi) \quad (3)$$

where  $\Phi$  is an arbitrary function,  $\Psi$  is the stream function,  $C$  is a constant to be evaluated later, and  $u_\tau$  is a function only of  $x$ .

Consider the continuity equation for compressible flow in cylindrical coordinates

$$\frac{\partial}{\partial x} (\rho u) + \frac{1}{r} \frac{\partial}{\partial r} (\rho v r) = 0 \quad (4)$$

from which a stream function can be defined by

$$\rho u r = \frac{\partial \Psi}{\partial r}; \quad \rho v r = - \frac{\partial \Psi}{\partial x} \quad (5)$$

Now if we invert the streamline hypothesis, equation 3 becomes

$$C\Psi = H(u/u_\tau) \quad (6)$$

which upon differentiation and insertion of equation 5 becomes

$$C \frac{1}{r} \frac{\partial \Psi}{\partial r} = C\rho u = \frac{1}{r} H' (u/u_\tau) \frac{1}{u_\tau} \frac{\partial u}{\partial r} \quad (7)$$

At a given value of x we can integrate equation 7 to obtain

$$\int_{r_0}^r u_\tau C \rho r dr = \int_0^{u/u_\tau} \frac{H'(u/u_\tau)}{u/u_\tau} d(u/u_\tau) \quad (8)$$

or

$$C u_\tau \int_{r_0}^r \rho r dr = G(u/u_\tau) \quad (9)$$

If we now invert the function G we have

$$\frac{u}{u_\tau} = F \left[ C u_\tau \int_{r_0}^r \rho r dr \right] \quad (10)$$

Using the Newtonian shear stress relation at the wall,

$$\tau_w = \mu_w (du/dr)_w \quad (11)$$

equation 10 implies

$$\begin{aligned} \left( \frac{du}{dr} \right)_{r=r_0} &= \frac{\tau_w}{\mu_w} \\ &= u_\tau \left\{ F' \left[ C u_\tau \int_{r_0}^r \rho r dr \right] C u_\tau \frac{d}{dr} \left[ \int_{r_0}^r \rho r dr \right] \right\}_{r=r_0} \end{aligned} \quad (12)$$

which reduces to

$$\frac{\tau_w}{\mu_w} = C u_\tau^2 F'(0) [\rho_w r_0] \quad (13)$$

Since  $C$  and  $F'(0)$  are both arbitrary constants we may, without loss of generality, set

$$F'(0) = 1 \quad (14)$$

and thus define

$$C = \frac{\tau_w}{\mu_w \rho_w u_\tau^2 r_0} \quad (15)$$

Therefore

$$\frac{u}{u_\tau} = F \left\{ \frac{\tau_w}{\mu_w \rho_w u_\tau^2 r_0} \int_{r_0}^r p r dr \right\} \quad (16)$$

As of this point  $u_\tau$  and  $F$  are undefined functions. In order to show the reduction of this relationship (equation 16) to the subsonic flat plate relationship (equation 1), it is convenient to define, following Coles (11),

$$\tau_w = \rho_\tau u_\tau^2 \quad (17)$$

where  $\rho_\tau$  is a "friction density" to be determined empirically. Furthermore, it is necessary that

$$F = f \quad (18)$$

where  $f$  is the well known empirically defined function of equation 1.

Thus equation 16 becomes

$$\frac{u}{u_{\tau}} = f \left\{ \frac{\rho_{\tau} u_{\tau}}{\mu_w \rho_w r_0} \int_{r_0}^r \rho r dr \right\} \quad (19)$$

That equation 19 reduces to the flat plate incompressible case can be shown by relaxing first the curvature restraint and then the compressibility restraint or vice versa.

To obtain the compressible flat plate similarity coordinates we can let  $r_0$  approach infinity. Keeping in mind that we are only interested in the region  $r \approx r_0$  as  $r_0$  approaches infinity, we can let  $r/r_0 = 1$  and  $dr = dy$  where  $y = r - r_0$ ; then

$$\frac{u}{u_{\tau}} = f \left[ \frac{\rho_{\tau} u_{\tau}}{\mu_w \rho_w} \int_0^y \rho dy \right] \quad (20)$$

To reduce this further to the incompressible flat plate case we set  $\rho = \rho_{\tau} = \rho_w = \text{constant}$  and obtain

$$\frac{u}{u_{\tau}} = f \left[ y \frac{u_{\tau}}{\nu} \right] \quad (21)$$

where  $\nu = \mu / \rho$ .

To obtain the incompressible similarity coordinates for flow on a cylinder we can set  $\rho = \rho_{\tau} = \rho_w = \text{constant}$  in equation 19 to yield

$$\frac{u}{u_{\tau}} = f \left[ \frac{u_{\tau}}{\nu} \frac{r^2 - r_0^2}{2r_0} \right] \quad (22)$$

Putting  $2r_0 = d$  and simplifying equation 22 we obtain

$$\frac{u}{u_{\tau}} = f \left[ \left( \frac{y u_{\tau}}{\nu} \right) \left( 1 + \frac{y}{d} \right) \right] \quad (23)$$

which clearly indicates the "stretching" of the coordinate  $y u_\tau / \nu$  in the case of axial incompressible flow on a cylinder. Note also that when  $d = \infty$  the flat plate coordinates are recovered.

In order to determine  $\rho_\tau$  for a particular supersonic boundary layer, both a local direct measurement of shear ( $\tau_w$ ) and a velocity profile must be obtained. Upon transforming the velocity profile to the coordinates of equations 19 or 20, depending upon the particular situation, a value of  $\rho_\tau / \rho_w$  can be obtained by fitting the transformed profile to the universal incompressible flat plate function  $f$  in the region near the wall. It has been found by Coles (11) that  $\rho_\tau / \rho_w$  is a function only of free stream Mach number for supersonic turbulent boundary layers on insulated flat plates. It will be shown later in this report that  $\rho_\tau / \rho_w$  for supersonic axial flow on a cylinder has the value found by Coles for a flat plate at the same Mach number.



### III. EXPERIMENTAL MODELS, INSTRUMENTATION, AND TECHNIQUES

#### A. Subsonic Facilities

##### 1) Merrill Wind Tunnel

A one-inch diameter aluminum tube 12 feet long was located along the geometrical flow axis of the low speed Merrill wind tunnel. The nose of the tube was located in the tunnel settling chamber at the screens and the aft end well within the tunnel test section as displayed in fig. 1. To survey the axial external flow on the cylinder a single traversing pitot mechanism was used which clamped onto the model, thereby eliminating discrepancies between pitot motion and model motion. At the lowest tunnel speed usable in keeping with the least count of the alcohol micro-manometer, the boundary layer was found to be turbulent. Therefore for subsequent runs only a relatively high tunnel speed was used to insure manometer accuracy. Thus turbulent boundary layer velocity profiles were obtained at 8, 9, and 10 feet from the nose of the cylinder with approximately 155 ft/sec test section free stream velocity. No measurement of boundary layer axial symmetry was made on this model.

##### 2) Low Turbulence Tunnel

A 0.024 inch diameter spring steel wire was installed parallel to the flow in the Low Turbulence tunnel as shown in fig. 2. The model was approximately 27 feet long of which the last 14 feet were in the uniform pressure test section of the tunnel. The wire fore end was draped over a pulley outside the intake of the tunnel and loaded in tension to 63 pounds ( $140,000 \text{ lbs/in}^2$ ) in order to maintain as straight as possible the horizontal portion of the model.

At this tensile stress the sag at the middle of a 23 foot length of wire would be approximately 0.020 inches. Approximately four feet from the rear of the wire model a vertical strut was located to move the rear of the model up, down, and to each side. With this strut and a double pitot sliding on and rotating about the wire model the boundary layer was forced to be symmetrical at the x station to be surveyed. The surveying instrument was a hot wire 0.0001 inches in diameter and 0.015 inches in span. The hot wire support was hinged to the same vertical strut so that much variation in distance between the hot wire and the wire model was eliminated. The hot wire was calibrated for mean flow by observing the shedding frequency of vortices in flow normal to a standardized cylinder. This method of calibration is nearly the only one possible at very low tunnel speeds when manometers are useless, and also is excellent at the higher speeds attainable in the present facility.

In addition to the above mentioned equipment a 10 foot long 8 inch diameter stovepipe was at times used in an attempt to align the flow around the model. Various boundary layer tripping devices were used on or near the wire model including a clay center-body on the model, a blunting rubber ring on the nose of the stovepipe, and a cross tunnel wire near the start of the test section. Laminar and turbulent boundary layers were distinguished by observing an oscilloscope trace of the hot wire output.

## B. Hypersonic Facility

Several cylinder models were installed and surveyed with pitot tubes in the GALCIT 5 x 5 inch hypersonic wind tunnel.

Because of the long model length required for naturally turbulent boundary layers and the desirability of using small diameter models to attain appreciable curvature effects, all models were supported from both ends in tension. Since a forward support in the supersonic tunnel flow would cause shock waves and a wake which might upset the boundary layer flow on the model, the forward support was located in the subsonic flow upstream of the tunnel throat. Therefore the models extended through the tunnel throat and their effect on the free stream flow had to be determined.

The three models shown in fig. 3 were used to determine the effect of their extension through the tunnel throat. Model 1 was 0.0625 inches in diameter for its entire length. Model 2 was 0.0625 inches in diameter through the throat and non-uniform supersonic expansion region and 0.250 inches in the test rhombus. The expansion was accomplished by a  $1.5^\circ$  half angle cone faired into the 0.250 inch size. Model 3 was 0.250 inches in diameter for its entire length except for notches at the tunnel throat. Free stream surveys were accomplished by an axially-traversing seven tube rake shown in fig. 3; the results are discussed in Section B1 of Part IV.

After determining the "model through the throat effect" a more detailed total head survey was made on the three models shown in fig. 4. Models 4 and 5 were 0.024 inches and 0.064 inches in diameter for their entire length. Model 6 was the same as model 2 except that a  $3^\circ$  half angle cone-ogive was used to reach the 0.250 inch size. Surveys were made axially and vertically with the 12

tube rake shown in fig. 4. Three tubes were located in each of four planes  $90^{\circ}$  apart around the models. The rear of each of the three cylinder models could be moved up and down from outside the tunnel while in operation, thus providing a means of making the boundary layer more symmetrical.

It was undertaken to construct a skin friction measuring device within a 0.250 inch cylinder. A first attempt was made by supporting a one-half inch long segment of the cylinder surface with split lock-washer type flexures and restraining it longitudinally with 0.0004 inch constantan strain wires at each end. This balance was marginal for sensitivity, was greatly affected by temperature gradients along the model, and proved wholly unsuccessful on tunnel starting due to the fragility of the strain wires.

A second, quite successful skin friction floating element balance was built within the 0.250 inch diameter segment of model number 7 shown in fig. 5. Externally, the floating element appeared as a 1/2 inch long segment of the 0.250 inch cylinder and was bounded by two 0.0025 inch gaps. As shown in fig. 5, a sliding shield with four pitot tubes attached was provided to protect the floating element on tunnel starting, to obtain zero force readings while the tunnel was hot and running, and to measure the axial symmetry of the boundary layer near the element station. The internal structure of the balance is shown in fig. 6. In order to support the entire model in tension a large structural member was required underneath the floating element. In the process of assembly this structural body was eventually pinned fore and aft

to the two segments of 0.250 inch stainless steel tubing. The floating element itself had a 0.005 inch thick wall. The floating components of the balance were located with respect to the fixed components by two split lock-washer type flexures shown in fig. 6. The flexures provided a quite rigid lateral support and an axial restraining spring force for the floating element. The spring force allowed a 0.001 inch longitudinal displacement of the element for a shear force of 500 milligrams. The floating element displacement was measured by determining the position of a magnetically conducting core within a transducer. The transducer was a center-tapped inductance coil wound on a thin stainless steel form and was excited by a 3 volt 31 kilocycle/second alternating-current voltage. In principle the inductance coil can be used as two legs of an alternating-current bridge, the other two being provided by a double resistance (potentiometer). Due to mis-matching of the bridge elements and internal capacitance to ground of the alternating-current instruments, it was found that a low enough A.C. null voltage to provide sufficient instrument sensitivity (least count) was unattainable. Therefore the electronic circuit of fig. 7 was developed. Essentially the small A.C. voltage was rectified and the resulting D.C. voltage read on a Leeds and Northrop potentiometer.

To calibrate the floating element a jewelled pulley was constructed whose support was clamped onto the 0.250 inch cylinder aft of the element. A single nylon fibre was attached to the floating element with hot wax, then draped over the pulley and loaded with a small pan and milligram weights. The break-out

force at the rim of the pulley was  $3/4$  milligram, a value quite small compared to the total of 500 milligrams applied during calibration. A typical calibration curve is shown in fig. 8. All calibrations resulted in a straight line which could be shifted horizontally to any desired position by the potentiometer  $R_5$  shown in fig. 7.

#### IV. EXPERIMENTAL RESULTS

##### A. Subsonic Flow

###### 1) Merrill Wind Tunnel

Turbulent boundary layer profiles were obtained from pitot surveys at three  $x$  stations on the one inch diameter cylinder. The data are presented in Table 1. The velocity profile at 9 feet is presented in fig. 9a in the usual coordinates and the one at 10 feet in the universal coordinates in fig. 9b. A turbulent skin friction coefficient can be estimated from fig. 9b with the aid of the streamline hypothesis as described in Appendix A. The computation of momentum thickness is described in Appendix B.

###### 2) Low Turbulence Tunnel

Turbulent boundary layer profiles were obtained on the 0.024 inch diameter cylinder 16 feet from the tunnel screens. Varying the boundary layer tripping mechanism resulted in only slight differences in the momentum thicknesses and estimated friction coefficients. Typical data are presented in Table 2. The profile obtained with a clay centerbody trip and flow aligning stovepipe is presented in two sets of coordinates in figs. 10a and 10b. All attempts to obtain a steady laminar boundary layer on the model proved futile. At very low tunnel speeds the boundary layer on the cylinder appeared to be laminar and stable (with respect to transition) but was quite non-steady with respect to position about the model. The boundary layer axial non-symmetry was found to be continually changing in an unpredictable manner.

A summary of properties of the subsonic experimental turbulent boundary layer is found in Table 3 and in figs. 11 and

12. To extend the results to negative curvature effects, Laufer's (reference 14) pipe flow results are included. In fig. 12 the estimated turbulent skin friction due to axial flow on (or in) a cylinder is compared to the flat plate value of Coles (10), the comparison always being taken at the same momentum thickness Reynolds number.

### B. Hypersonic Flow

#### 1) Effect of Models Extending Through the Tunnel Throat

A rake survey showed no noticeable effect on the test rhombus free stream flow when a long 0.0625 inch cylinder extended through the flow expansion region and tunnel throat. Similarly, the free stream flow was unaffected by the composite 0.0625 and 0.250 inch model except for the very weak shock wave generated by the model conical expansion. The 0.250 inch cylinder contoured to fit the tunnel throat, however, seriously distorted the test rhombus flow and therefore was not tested further.

#### 2) Alignment of the Models and Pitot Surveys

Complete axial surveys were made with the 12 pitot rake on the 0.024 inch, 0.064 inch, and on the composite 0.0625 and 0.250 inch cylinder. On all models the side boundary layer thicknesses were smaller than the top and bottom thicknesses. This effect was most pronounced at  $x = 10$  to 12 inches from the tunnel throat where the tunnel side-wall throat waves cross the model.\* Downstream of this point the axial symmetry steadily improved and was quite good at 24 inches. However, due to the presence of weak free stream waves at  $x = 24$  inches, the final pitot surveys

---

\*For further discussion of the throat waves see p. 98 of Ref. 16.



were obtained at  $x = 20$  inches where the boundary layer was nearly symmetrical. A correction factor of from 0.842 to 0.866, depending on the free stream Reynolds number per inch, was applied to the momentum and displacement thicknesses as computed from the thicker boundary layer on top of the models.

In the hypersonic facility laminar and naturally turbulent boundary layers were found on all models tested. Typical raw data for three model sizes are presented in Table 4. Boundary layer profile plots are presented in figs. 13 to 18b inclusive. Included on the plots are the wall slopes as determined from measured laminar and turbulent shear on the 0.250 inch model, and estimated turbulent shear on the 0.064 inch and 0.024 inch models. The method of estimating turbulent skin friction from velocity profiles is described in Appendix A. The data reduction methods are described in Appendix C.

The computed Reynolds number based on average momentum thickness around the 0.250 inch cylinder at  $x = 20$  inches is presented in fig. 19 for various tunnel reservoir pressures. It is believed that the computed point at  $P_0 = 24.4 \text{ lbs/in}^2$  is in error due to difficulty in estimating the free stream properties from the measured pitot profile; at this tunnel pressure the free stream pitot pressure at the outer edge of the boundary layer was not uniform, as evidenced from the profile presented in Table 4. Therefore the estimated point represented by the broken circle was used in all subsequent charts and tables. Further discussion can be found in Appendix B.

### 3) Measured Skin Friction on the 0.250 inch Cylinder

Fig. 20 is a plot of measured wall friction on the 0.250 inch model by use of the floating element balance located within the model 20 inches from the tunnel throat. It will be noted that laminar, transitional, and turbulent values were obtained. The repeatability of duplicate points taken on different days is seen to be excellent, being within  $\pm 1.25$  percent of the average. The dash-pot contained air only, at a pressure equal to the floating element gap static pressure.

A summary of the measured laminar and turbulent skin friction on the 0.250 inch model and the estimated turbulent skin friction on the 0.064 and 0.024 inch models is presented in Table 5 and Table 6 and in fig. 21. Fig. 22 presents a comparison of laminar skin friction on a cylinder with the laminar flat plate value of Van Driest (reference 15) and turbulent skin friction on a cylinder with the turbulent flat plate value of Korkegi (reference 16). All comparisons were made at the same momentum thickness Reynolds number. Included in fig. 22 is the incompressible laminar theory of Glauert and Lighthill and an extension to compressible flow as described in Appendix D.

## V. CONCLUSIONS

Steady, thick, subsonic axially symmetric laminar boundary layers on cylinders are difficult to obtain experimentally.

Steady, thick, supersonic axially symmetric laminar boundary layers are obtainable experimentally and indicate laminar skin friction several times that on a flat plate at the same Mach number and momentum thickness Reynolds number.

The skin friction associated with an axially symmetric subsonic turbulent boundary layer on a cylinder can be substantially greater than that on a flat plate at the same momentum thickness Reynolds number. The turbulent skin friction appears to approach an asymptotic value as  $\theta/d$ , the transverse curvature parameter, becomes arbitrarily large.

At  $M_1 = 5.8$ , the skin friction due to an axially symmetric turbulent boundary layer on a cylinder can be double that for a flat plate at the same Mach number and momentum thickness Reynolds number.

The effect of transverse curvature on both laminar and turbulent skin friction is larger, the higher the free stream Mach number.

REFERENCES

1. Seban, R. A., and Bond, R., "Skin Friction and Heat Transfer Characteristics of a Laminar Boundary Layer on a Cylinder in Axial Incompressible Flow", J. Aero. Sci., V. 18, p. 671 (1951).
2. Kelly, H. R., "A Note on the Laminar Boundary Layer on a Circular Cylinder in Axial Incompressible Flow", J. Aero. Sci., V. 21, p. 634 (1954).
3. Moore, F. K., "Displacement Effect of a Three Dimensional Boundary Layer", N.A.C.A. TN 2722 (1952).
4. Cooper, R. D., and Tulin, M. P., "The Laminar Flow About Very Slender Cylinders in Axial Motion, Including the Effect of Pressure Gradients and Unsteady Motions", D. W. Taylor Model Basin Rep. 838 (1953).
5. Glauert, M. B., and Lighthill, M. J., "The Axisymmetric Boundary Layer on a Long Thin Cylinder", Royal Soc. of London Proceedings, V. 230, p. 188 (1955).
6. Stewartson, K., "The Asymptotic Boundary Layer on a Circular Cylinder", Quart. Appl. Math., July 1955.
7. Mark, R. M., "Laminar Boundary Layers on Slender Bodies of Revolution in Axial Flow", GALCIT Hypersonic Wind Tunnel Memorandum No. 21 (1954).
8. Probstein, R. F., and Elliott, D., "The Transverse Curvature Effect in Compressible Axially Symmetric Laminar Boundary Layer Flow", J. Aero. Sci., V. 23, p. 208, March 1956.
9. Eckert, Hans U., "Simplified Treatment of the Turbulent Boundary Layer Along a Cylinder in Compressible Flow", J. Aero. Sci., V. 19, p. 23, (1952).

10. Coles, D., "The Problem of the Turbulent Boundary Layer", ZAMP, V 5, N 3, p. 181 (1954).
11. Coles, D., "The Law of the Wall in Turbulent Shear Flow", 50 Jahre Grenzschichtforschung (ed. by Görtler and Tollmien), F. Vieweg und Sohn, Braunschweig, p. 153 (1955).
12. Coles, D., "The Law of the Wake in the Turbulent Boundary Layer", J. of Fluid Mech., V. 1, Pt. 2, p. 191, July 1956.
13. Coles, D., "Remarks on the Equilibrium Turbulent Boundary Layer", GALCIT Miscellaneous Publication, June 1956.
14. Laufer, J., "The Structure of Turbulence in Fully Developed Pipe Flow", NACA TN 2954 (1953).
15. Van Driest, E. R., "The Laminar Boundary Layer with Variable Fluid Properties", Heat Transfer and Fluid Mechanics Institute, Univ. of Calif. at Berkeley, p. 127 (1954).
16. Korkegi, R. H., "Transition Studies and Skin Friction Measurements on an Insulated Flat Plate at a Mach Number of 5.8", J. Aero. Sci., V. 23, p. 97 (1956).

## APPENDIX A

### Estimation of Turbulent Skin Friction from a Velocity Profile

#### 1) Subsonic Flow

Starting with the experimental boundary layer values of  $u$  and  $y$  near a cylinder model, a value of  $u_\tau$  was determined which would cause the variables  $u/u_\tau$  and  $(yu_\tau/\nu)(1 + y/d)$  near the wall to fit the universal flat plate function given by Coles (10). From this value of  $u_\tau$  the friction coefficient was computed according to

$$C_f = \frac{\tau_w}{q} = \frac{\rho u_\tau^2}{\frac{1}{2} \rho_1 u_1^2} = 2 \left( \frac{u_\tau}{u_1} \right)^2$$

#### 2) Hypersonic Flow

Starting with the experimental and computational values of  $\rho/\rho_w$  and  $r$  near the wall of a cylinder model evaluation at each data point of

$$\int_{r_0}^r \rho/\rho_w \, r dr$$

was made. It was assumed that  $\rho_\tau/\rho_w = 1.74$  at  $M_1 = 5.8$  (the flat plate value) for the cylinder.  $U_\tau$  was estimated and the variables

$$u/u_\tau \quad \text{and} \quad \frac{\rho_\tau u_\tau}{\mu_w r_0} \int_{r_0}^r \frac{\rho}{\rho_w} \, r dr$$

plotted on the same universal subsonic flat plate curve of Coles (10). At times a re-estimation of  $u_\tau$  was necessary. Note that  $\mu_w$  and  $\rho_w$ , the wall values of viscosity coefficient and density, must be determined at the actual wall recovery temperature, and not at the free stream stagnation temperature. The local turbulent

skin friction coefficient was then computed from

$$C_f = \frac{\tau_w}{q} = \frac{\rho_\tau u_\tau^2}{\frac{1}{2} \rho_1 u_1^2} = 2 \frac{\rho_\tau}{\rho_1} \left( \frac{u_\tau}{u_1} \right)^2$$

Invariably, values of  $u$  near a wall in a compressible boundary layer as determined from pitot pressures are too high. Therefore after estimating the wall shear and hence the wall slope of the velocity profile, a much more reasonable value of  $u$  was estimated from the relation

$$\tau_w = \mu_w (u/y) \text{ near the wall}$$

Such estimated velocities are represented by the doubly flagged circles in figs. 14b, 16b, and 18b.

## APPENDIX B

### Relationships for Determination of Displacement and Momentum Thicknesses

The boundary layer momentum thickness which physically corresponds to that on a flat plate is defined by

$$\int_{r_0}^{\theta+r_0} \rho_1 u_1^2 2\pi r dr = \int_{r_0}^{\delta+r_0} \rho u(u_1-u) 2\pi r dr$$

or

$$(\theta+r_0)^2 - r_0^2 = \int_{r_0}^{\delta+r_0} \frac{\rho u}{\rho_1 u_1} \left(1 - \frac{u}{u_1}\right) d(r^2)$$

Similarly the displacement thickness is defined by

$$(\delta^*+r_0)^2 - r_0^2 = \int_{r_0}^{\delta+r_0} \left(1 - \frac{\rho u}{\rho_1 u_1}\right) d(r^2)$$

The incompressible definitions can be obtained by merely setting  $\rho/\rho_1 = 1$ .

In the right hand integral of the above expressions the additional  $r$  appearing results in a greater contribution to mass or momentum defect from the outer regions of an axially symmetric boundary layer than would be obtained for a flat plate boundary layer. Therefore the computed values of  $\delta^*$  and  $\theta$  are greatly affected by the choice of free stream velocity and boundary layer thickness. In addition the choice of free stream velocity and boundary layer thickness is more difficult than for a flat plate due to the added fullness of the axially symmetric boundary layer velocity profile. This



problem is slightly lessened for the supersonic boundary layer if we choose the free stream quantities and boundary layer thickness from a Mach number profile rather than a velocity profile as may be evidenced from figs. 13 through 18.

## APPENDIX C

### Supersonic Boundary Layer

#### Flow Data Reduction Methods

The measured data included  $P_0$  and  $T_0$ , the tunnel reservoir pressure and temperature, and a profile of  $y$  versus  $P_0'$ , the pitot pressure in the boundary layer and free stream.

By assuming isentropic free stream tunnel flow the free stream Mach number was obtained and thus the free stream static pressure and temperature determined. By using Rayleigh's pitot formula and by assuming constant static pressure through the boundary layer a Mach number profile was obtained. Then assuming a constant  $T_0$  through the boundary layer (i. e. an adiabatic relationship between  $M$  and  $T$  in the boundary layer) and the perfect gas law, density, temperature, and velocity profiles were obtained. Free stream Reynolds number per inch was computed by assuming Sutherland's viscosity law holds even at the low free stream temperatures obtained ( $90^\circ$  Rankine).

For determination of the wall values of the flow variables assumed temperature recovery factors of 0.9 for the turbulent and 0.86 for the laminar boundary layer were employed. The wall viscosity was then determined from Sutherland's viscosity law

$$\mu_w = \frac{2.27 \times 10^{-8} T_w^{3/2}}{T_w + 198.6} \quad \text{lb sec/ft}^2$$

where  $T_w$  is in degrees Rankine. To determine the wall velocity slope or Mach number slope from the measured or estimated wall shear the following simple relations were used:

$$\tau_w = \mu_w \left( \frac{du}{dr} \right)_w$$

$$\left[ \frac{dr}{d(u/u_1)} \right]_w = \frac{u_1}{(du/dr)_w}$$

$$\left[ \frac{dr}{d(M/M_1)} \right]_w = \sqrt{\frac{T_w}{T_1}} \left[ \frac{dr}{d(u/u_1)} \right]_w$$

## APPENDIX D

### Reduction of Laminar Theory to Local Properties

Inherent in all of the laminar theories of Part I of this paper is the quantity  $x$ . Since there is no definable  $x$  for the present experiments, comparison with theory can only be accomplished by elimination of  $x$  from them.

In principle, at least for most of the theories mentioned, the boundary layer momentum thickness,  $\theta$ , can be found as a unique function of  $x$ , thus permitting evaluation of the friction coefficient,  $C_f$ , as a function only of the local property  $\theta$ . Fortunately (for the present purpose) Glauert and Lighthill (5) have tabulated their results in such a way that discrete values of  $C_f$  and  $\theta$  are immediately obtainable. The necessary transformations from the notation of reference 5 to the present notation are:

Ref. 5 Notation

Present Notation

$$\frac{F}{\mu U}$$



$$\frac{\pi}{\theta/r_0} R_{\theta} C_f$$

$$\frac{\frac{\pi}{2}}{\pi a}$$



$$\left(\frac{\theta}{r_0} + 1\right)^2 - 1$$

The resulting curve of  $C_f/C_f$  (flat plate) versus  $\theta/d$  for incompressible laminar flow is presented in fig. 22.

Coles, in a private communication, noted that a simple transformation of the compressible flow variables would allow extension of the incompressible Glauert-Lighthill solution to the compressible case. The transformation is

$$\rho r dr = \rho_w \bar{r} d\bar{r}$$

The new variable  $\bar{r}$  can have limits similar to those for  $r$  if we choose an integration constant such that

$$\bar{r}^2 = r_0^2 + 2 \int_{r_0}^r \frac{\rho}{\rho_w} r dr$$

The assumed velocity profile in the new variables is

$$\frac{u}{u_1} = \frac{\ln(\bar{r}/r_0)}{a_c}$$

which is quite similar to that used by Mark (7), and reduces exactly to the Glauert-Lighthill profile for incompressible flow. It can easily be shown that the Glauert-Lighthill tabulated incompressible quantities have the same mutual relationships as the transformed quantities noted below.

Ref. 5 Incomp. Notation		Ref. 5 Comp. Notation		Present Comp. Notation
$\frac{F}{\mu U}$	$\longrightarrow$	$\frac{F}{\mu_w U}$	$\longrightarrow$	$(\mu_w/\mu_1)(\theta/r_0) C_f R_\theta$
$\frac{(\Theta)}{\pi a^2}$	$\longrightarrow$	$\frac{(\Theta)}{\pi a^2}$	$\longrightarrow$	$\frac{\rho_1}{\rho_w} [(\frac{\theta}{r_0} + 1)^2 - 1]$
$\frac{\nu_x}{U a^2}$	$\longrightarrow$	$\frac{\nu_w^x}{U a^2}$	$\longrightarrow$	$\frac{\nu_w^x}{u_1 r_0^2}$

The resulting  $C_f/C_f$  (flat plate) versus  $\theta/d$  is plotted in fig. 22.

The following table is taken from Glauert-Lighthill with the above transformations included.

Incompressible			(M <sub>1</sub> = 5.8) Compressible		
$\theta/d$	$C_f R_\theta$	$\frac{C_f}{C_{f(\text{Flat Plate})}}$	$\theta/d$	$C_f R_\theta$	$\frac{C_f}{C_{f(\text{Flat Plate})}}$
.0108	.4864	1.012	.00141	.4913	1.021
.0190	.4938	1.028	.00249	.5003	1.040
.0350	.5470	1.13	.00467	.5647	1.18
.0648	.6390	1.33	.00884	.6743	1.40
.1199	.7633	1.59	.01708	.8405	1.75
.2240	.9868	2.05	.03432	1.169	2.43
.4151	1.324	2.76	.0709	1.749	3.64
.762	1.887	3.93	.1509	2.889	6.02
1.364	2.683	5.58	.3168	4.817	9.25
2.355	3.762	7.83	.628	7.756	16.1
4.036	5.369	11.2	1.197	12.31	25.6
7.33	8.305	17.3	2.677	23.45	48.8
11.5	11.35	23.6	4.343	33.13	69.0

In the above tabulation  $R_\theta C_f$  (flat plate) was taken as the Blasius value, 0.4409, plus 9<sup>o</sup>o.

An attempt was made to examine compressible laminar skin friction on a cylinder by deriving a velocity profile which would identically satisfy the energy integral, the transport terms in the momentum equation being neglected. The resulting  $C_f R_\theta$  at particular  $\theta/d$  values was considerably lower than that above.

Table 1

Merrill Wind Tunnel Turbulent Boundary Layer  
Velocity Profile Data

Free stream velocity  $= u_1 = 154$  ft/sec

Model diameter  $= 1.0$  inches

Distance from tunnel screens  $= x$

y (inches)	x = 8 feet $u/u_1$	x = 9 feet $u/u_1$	x = 10 feet $u/u_1$
0.02	.611	.581	.574
0.04	.691	.662	.661
0.06	.732	.694	.688
0.08	.759	.728	.725
0.10	.788	.755	.750
0.145	.821	.794	.793
0.19	.868	.833	.816
0.23	.887	.860	.844
0.27	.912	.885	.864
0.35	.949	.924	.902
0.44	.971	.949	.925
0.52	.984	.965	.952
0.69	.998	.984	.972
0.85	1.000	.998	.987
1.105	1.001	1.000	.998
1.27	1.000	1.000	.998
1.435	1.001	1.000	1.000
1.605	0.999	1.002	1.000

Table 2

Low Turbulence Tunnel Turbulent Boundary Layer  
Velocity Profile Data

Model Diameter = 0.024 inches

Distance from Tunnel Screens = 16 feet

y (inches)	u (cm/sec)	y (inches)	u (cm/sec)	y (inches)	u (cm/sec)	y (inches)	u (cm/sec)
0.006	490	0.012	625	0.012	684	0.009	149
0.009	570	0.015	746	0.015	730	0.012	172
0.012	690	0.018	831	0.018	822	0.015	200
0.015	805	0.021	891	0.021	882	0.018	236
0.018	864			0.024	917	0.021	262
0.021	910	0.027	950	0.027	955	0.024	275
0.024	945					0.027	300
0.027	970	0.042	1020	0.033	994	0.030	313
0.030	988	0.057	1052				
		0.072	1065	0.042	1032	0.045	351
0.036	1023	0.087	1083	0.057	1075	0.060	376
0.042	1042	0.102	1096	0.072	1096	0.075	386
				0.087	1117	0.090	395
0.057	1070	0.132	1110				
0.072	1091	0.147	1118	0.117	1139	0.120	409
0.087	1107						
0.102	1119	0.177	1122	0.162	1162	0.165	420
		0.207	1139	0.237	1183	0.240	430
0.177	1145			0.312	1201	0.315	439
0.252	1160	0.252	1151				
0.327	1173			0.462	1219	0.465	440
		0.327	1161	0.612	1230	0.615	448
0.477	1191	0.477	1182	0.762	1232	0.765	455
0.627	1209	0.627	1196	0.912	1238	0.915	459
0.777	1220	0.777	1201	1.062	1239	1.065	459
0.927	1230	0.927	1211				
1.077	1240	1.077	1219				
Natural Transition		Clay Center- body Trip		Clay Centerbody Trip and Stovepipe		Clay Centerbody Trip and Stovepipe	



Table 3

## Summary of Subsonic Turbulent Boundary Layer Curvature Effects

$M_1$	d (inches)	$\delta^*$ (inches)	$\theta$ (inches)	$\theta/d$	$R_\theta$	$C_f$	$C_f/C_f^f$ (flat plate)	Reference
0.089	9.72		-0.268	-0.0276	13,750	0.00247	1.037	Laufer Pipe (Ref. 14) Friction by Pressure Drop
0.1375	1.00	0.085	0.069	0.069	5,540	0.00323	1.15	Merrill Wind Tunnel Estimated Skin Friction
	1.00	0.109	0.094	0.094	7,540	0.00305	1.15	
	1.00	0.125	0.109	0.109	8,750	0.00290	1.13	
0.036	0.024	0.123	0.0995	4.15	2,100	0.00495	1.47	Low Turbu- lence Tunnel Estimated Skin Friction
	0.024	0.140	0.135	5.6	2,800	0.00518	1.61	
	0.024	0.162	0.156	6.5	3,310	0.00518	1.67	
0.014	0.024	0.109	0.122	5.1	954	0.00592	1.50	

 $\dagger C_f$ (flat plate) due to Coles (Ref. 10)

 $\delta^*$  and  $\theta$  are defined in Appendix B

Table 4

Hypersonic Boundary Layer Profile Data

Distance from Tunnel Throat = 20 inches

Model Diameter = 0.024 inches

Turbulent		Laminar	
r (inches)	M	r (inches)	M
0.017	1.72	0.017	1.48
0.035	2.79	0.035	1.81
0.053	3.72	0.053	2.24
0.072	4.04	0.072	2.52
0.090	4.27	0.090	2.76
0.108	4.49	0.108	3.02
0.144	4.84	0.126	3.21
0.180	5.14	0.144	3.51
0.217	5.41	0.163	3.78
0.254	5.62	0.181	4.11
0.290	5.73	0.199	4.47
0.331	5.78	0.217	4.81
0.372	5.79	0.235	5.10
0.408	5.80	0.254	5.31
0.445	5.82	0.272	5.43
0.481	5.82	0.290	5.51
0.517	5.83	0.308	5.54
0.554	5.83	0.333	5.58
0.572	5.83	0.357	5.33
$P_0 = 84.35 \text{ psia}$		$P_0 = 24.4 \text{ psia}$	
$T_0 = 225^\circ \text{ F}$		$T_0 = 225^\circ \text{ F}$	

Table 4 (Cont'd)

Model Diameter = 0.064 inches

Turbulent		Laminar	
r (inches)	M	r (inches)	M
0.037	0.92	0.037	1.02
0.046	1.31	0.055	1.02
0.055	2.31	0.073	1.13
0.064	2.88	0.092	1.44
0.073	3.19	0.110	1.99
0.092	3.51	0.128	2.61
0.110	3.79	0.146	3.36
0.128	4.01	0.164	4.08
0.164	4.36	0.183	4.59
0.201	4.66	0.201	4.95
0.237	4.92	0.219	5.15
0.274	5.14	0.237	5.29
0.310	5.32	0.255	5.47
0.335	5.41	0.274	5.62
0.359	5.50	0.292	5.72
0.396	5.63	0.310	5.75
0.432	5.74	0.336	5.75
0.468	5.78	0.363	5.74
0.505	5.79	0.381	5.74
0.541	5.79	0.399	5.74
0.559	5.79	0.417	5.74

$P_0 = 84.4$  psia

$T_0 = 225^\circ$  F

$P_0 = 24.4$  psia

$T_0 = 225^\circ$  F

Table 4 (Cont'd)

Model Diameter = 0.250 inches

Turbulent				Laminar			
r (inches)	M	r (inches)	M	r (inches)	M	r (inches)	M
0.130	1.12	0.130	0.91	0.130	0.96	0.130	1.27
0.142	1.41	0.142	1.10	0.157	1.12	0.152	1.31
0.152	1.97	0.152	1.95	0.182	1.24	0.177	1.35
0.162	2.48	0.162	2.45	0.207	1.43	0.202	1.50
0.172	2.82	0.172	2.80	0.232	1.67	0.227	1.64
0.182	3.02	0.182	3.03	0.257	2.03	0.252	1.89
0.207	3.41	0.207	3.42	0.282	2.61	0.277	2.20
0.232	3.73	0.232	3.67	0.295	2.97	0.302	2.48
0.257	3.99	0.257	4.01	0.307	3.39	0.327	2.92
0.282	4.26	0.282	4.29	0.320	3.90	0.352	3.54
0.307	4.52	0.307	4.57	0.332	4.33	0.377	4.31
0.332	4.76	0.332	4.84	0.345	4.64	0.402	4.84
0.357	5.05	0.357	5.10	0.357	4.83	0.427	5.09
0.382	5.24	0.382	5.32	0.370	4.96	0.477	5.40
0.407	5.44	0.407	5.49	0.382	5.06	0.527	5.53
0.432	5.60	0.432	5.61	0.407	5.19	0.577	5.54
0.457	5.68	0.457	5.68	0.432	5.35	0.627	5.60
0.482	5.73	0.482	5.73	0.457	5.43		
0.507	5.77	0.507	5.75	0.482	5.51		
0.532	5.77	0.532	5.75	0.507	5.58		
0.557	5.78	0.557	5.75	0.532	5.67		
0.582	5.78	0.582	5.75	0.557	5.72		
				0.582	5.61		
				0.607	5.59		
				0.632	5.58		
$P_0 = 84.4$ psia		$P_0 = 64.45$ psia		$P_0 = 24.45$ psia		$P_0 = 14.45$ psia	
$T_0 = 225^{\circ}$ F		$T_0 = 225^{\circ}$ F		$T_0 = 225^{\circ}$ F		$T_0 = 202^{\circ}$ F	

Table 5

## Summary of Hypersonic Laminar Boundary Layer Curvature Effects

$M_1$	d (inches)	$\delta^*$ (inches)	$\theta$ (inches)	$\theta/d$	$R_\theta$	$C_f$	$C_f / C_f^\dagger$ (flat plate)	
5.560	0.250	0.1767	0.0170	0.068	930	0.00150	3.32	GALCIT 5x5 inch Hypersonic Tunnel Measured Skin Friction
5.595	0.250	0.2040	0.0210	0.084	862	0.00230	4.76	
5.75	0.064	0.1267	0.0178	0.278	1102	-		
5.595	0.024	0.1422	0.0304	1.265	2000	-		

$\dagger C_f$  (flat plate) due to Van Driest (Ref. 15)

$\delta^*$  and  $\theta$  are defined in Appendix B

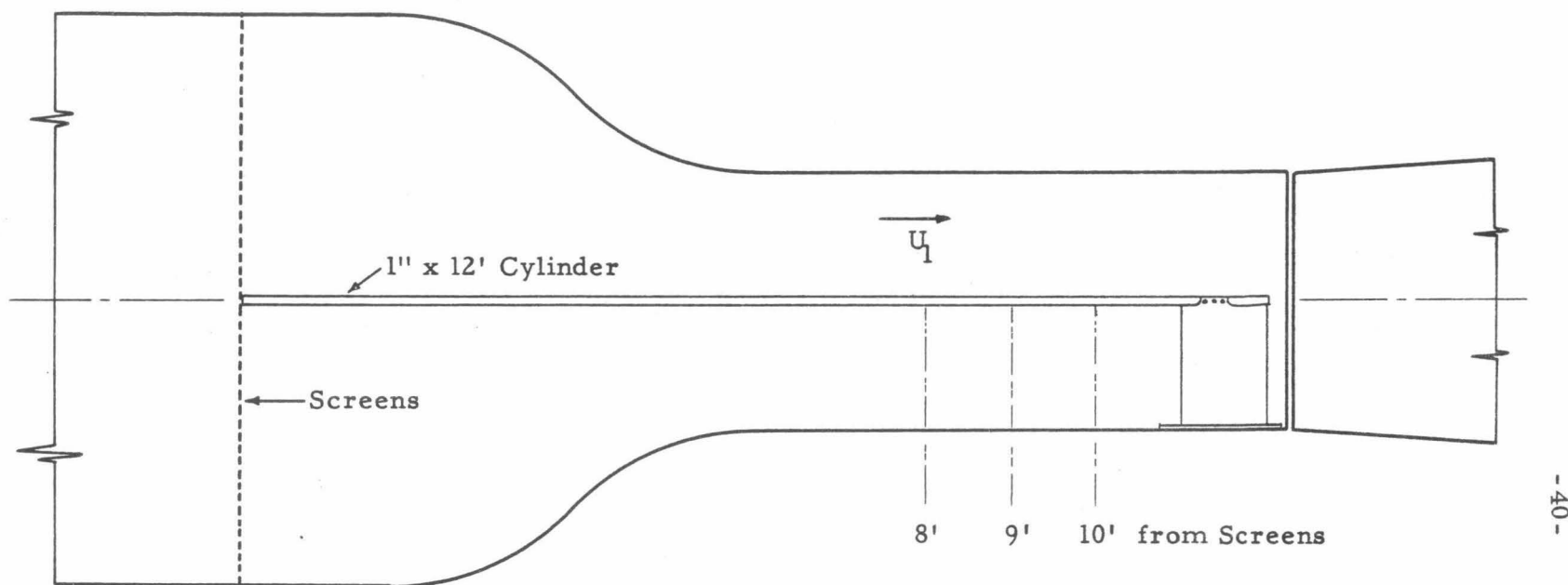
Table 6

## Summary of Hypersonic Turbulent Boundary Layer Curvature Effects

$M_i$	d (inches)	$\delta^*$ (inches)	$\theta$ (inches)	$\theta/d$	$R_\theta$	$C_f$	$C_f/C_f^\dagger$ (flat plate)	
5.785	0.250	0.1355	0.0158	0.0540	2850	0.00185	1.45	GALCIT 5x5 inch
5.775	0.250	0.1350	0.0162	0.0544	2540	0.00194	1.47	Hypersonic Tunnel
5.760	0.250	0.1337	0.0152	0.0524	2140	0.00203	1.48	Measured Skin Friction
5.80	0.064	0.1461	0.0246	0.384	5170	0.00213	1.94	Estimated Skin Friction
5.825	0.024	0.1062	0.0210	0.875	4390	0.00234	2.04	Estimated Skin Friction

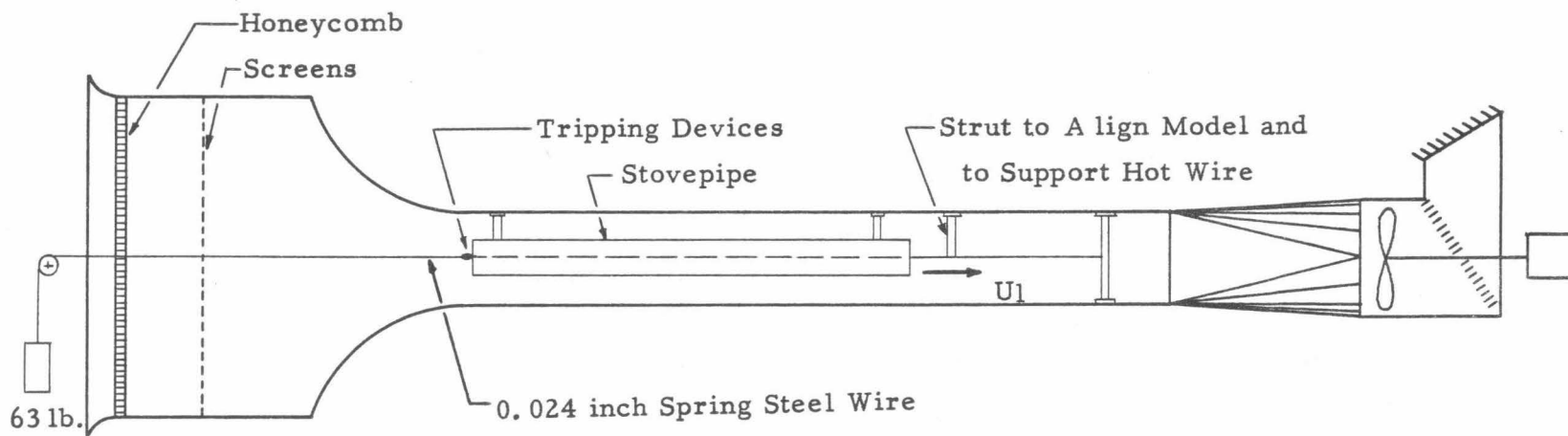
$^\dagger C_f$  (flat plate) due to Korkegi (Ref. 16)

$\delta^*$  and  $\theta$  are defined in Appendix B



SCHEMATIC DIAGRAM OF 1" DIAMETER CYLINDER INSTALLATION IN THE  
MERRILL WIND TUNNEL

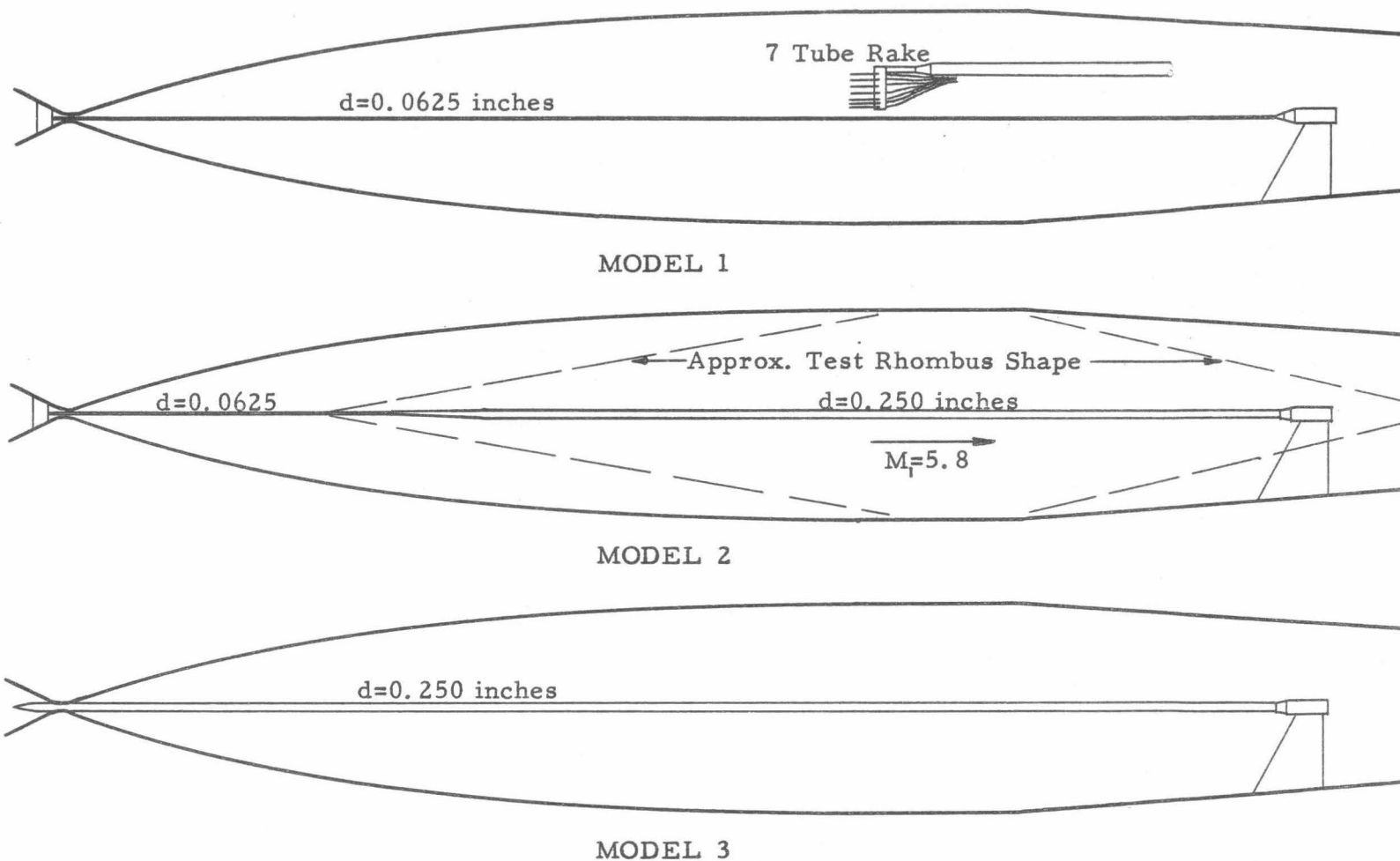
FIGURE 1



SCHEMATIC DIAGRAM OF THE 0.024 INCH WIRE MODEL INSTALLATION  
IN THE LOW TURBULENCE TUNNEL

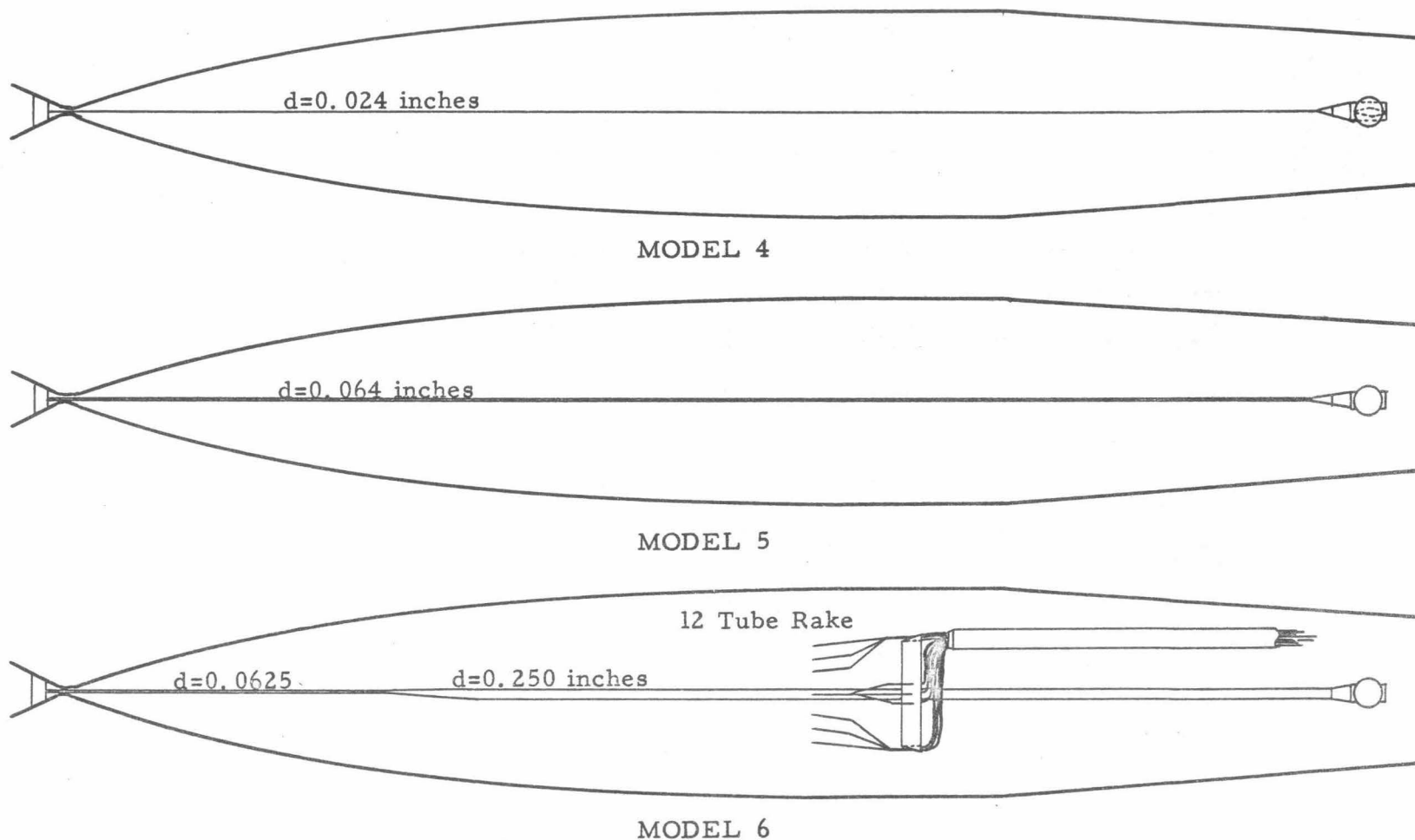
FIGURE 2





SCHEMATIC DIAGRAM OF CYLINDER MODELS IN THE 5x5 INCH HYPERSONIC TUNNEL

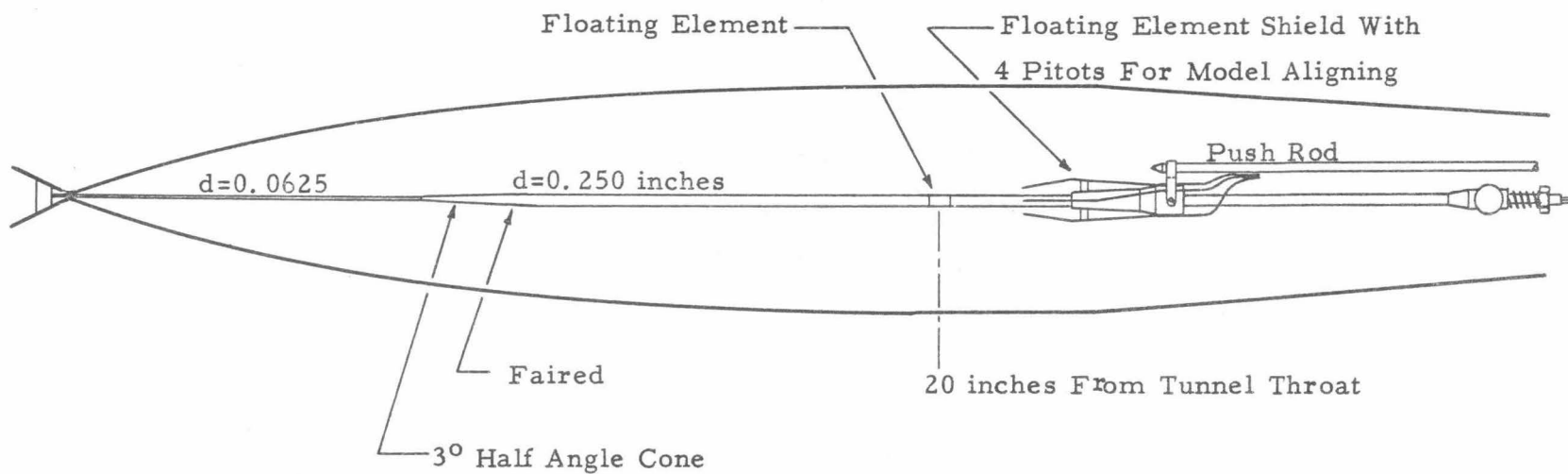
FIGURE 3



-43-

SCHEMATIC DIAGRAM OF CYLINDER MODELS IN THE 5x5 INCH HYPERSONIC TUNNEL

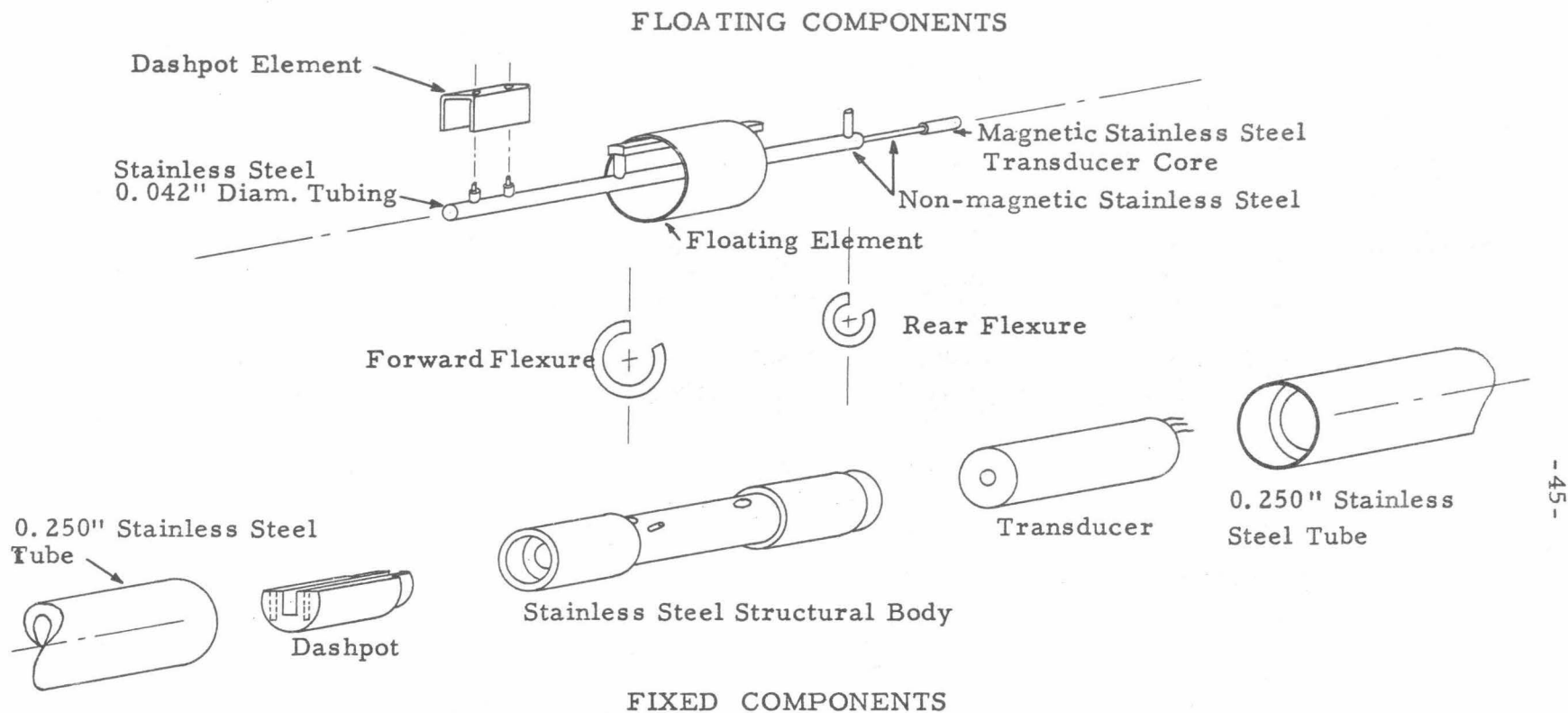
FIGURE 4



-44-

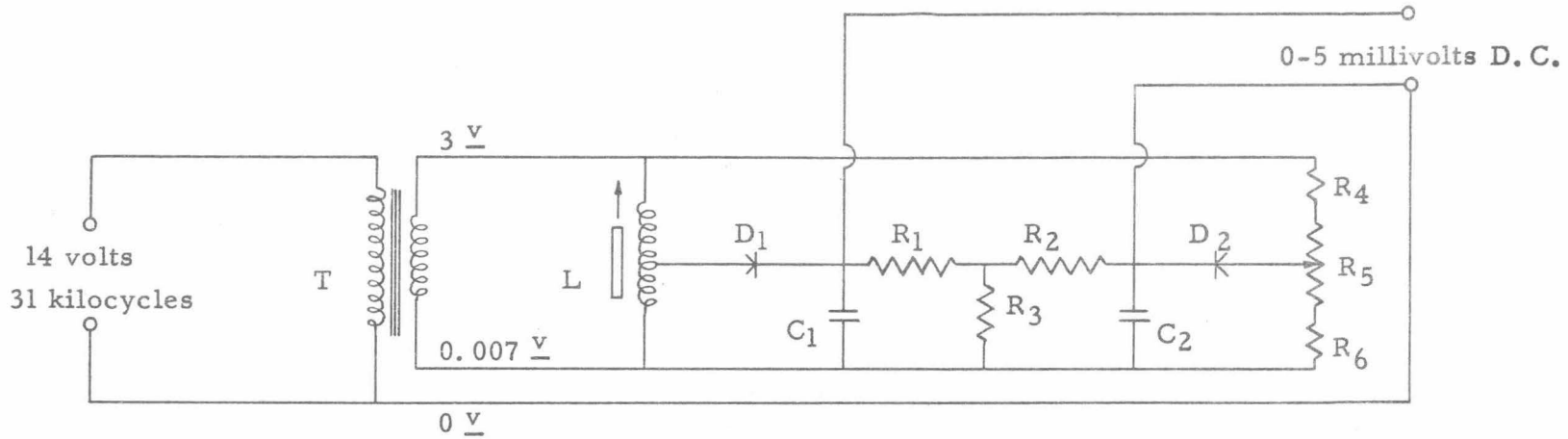
SCHEMATIC DIAGRAM OF THE 0.250 INCH SKIN FRICTION MODEL AND STARTING SHIELD  
IN THE 5x5 INCH HYPERSONIC TUNNEL

FIGURE 5



CABINET DRAWING OF THE 0.250 INCH SKIN FRICTION MODEL FLOATING ELEMENT MECHANISM

FIGURE 6

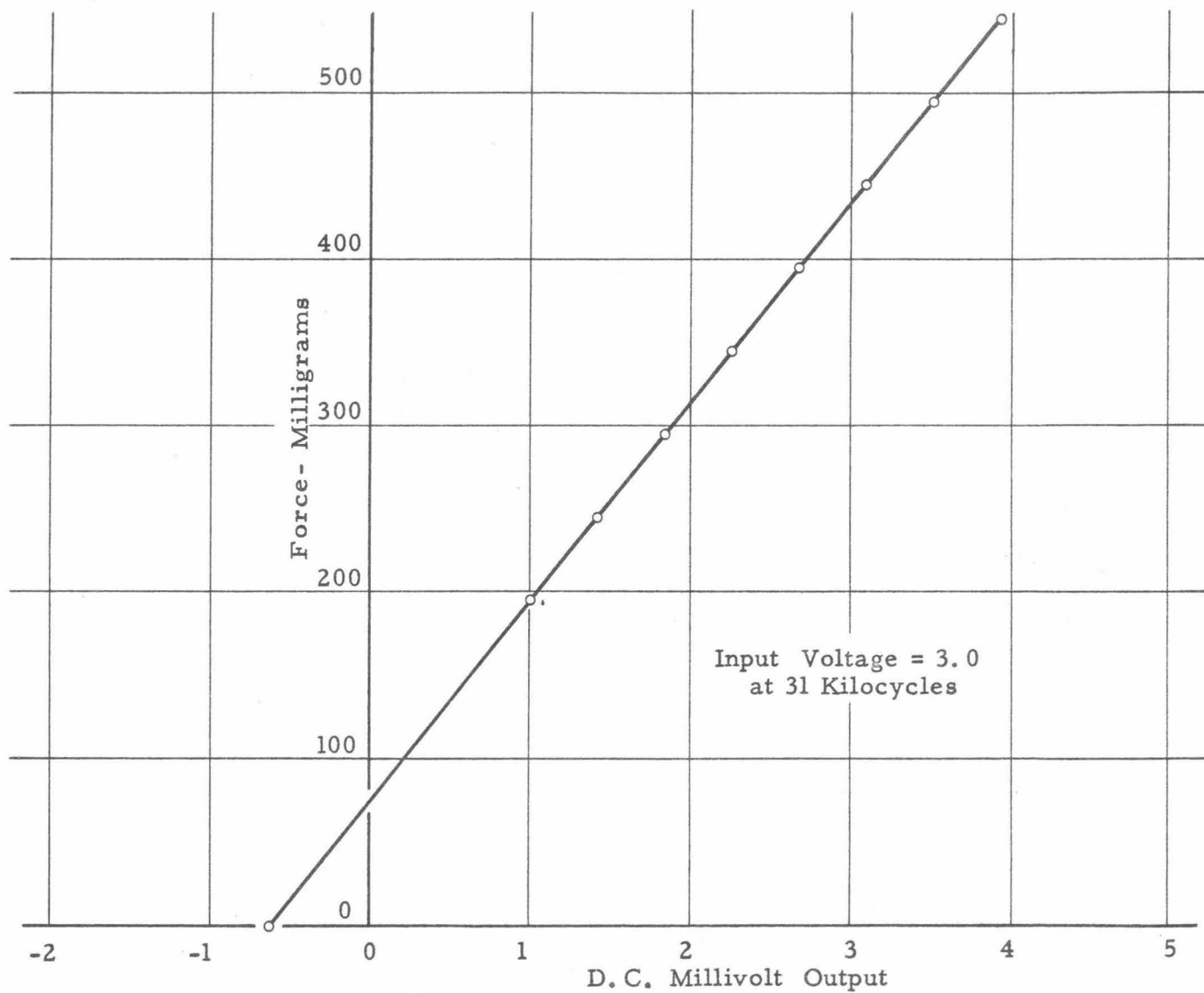


#### SPECIFICATIONS:

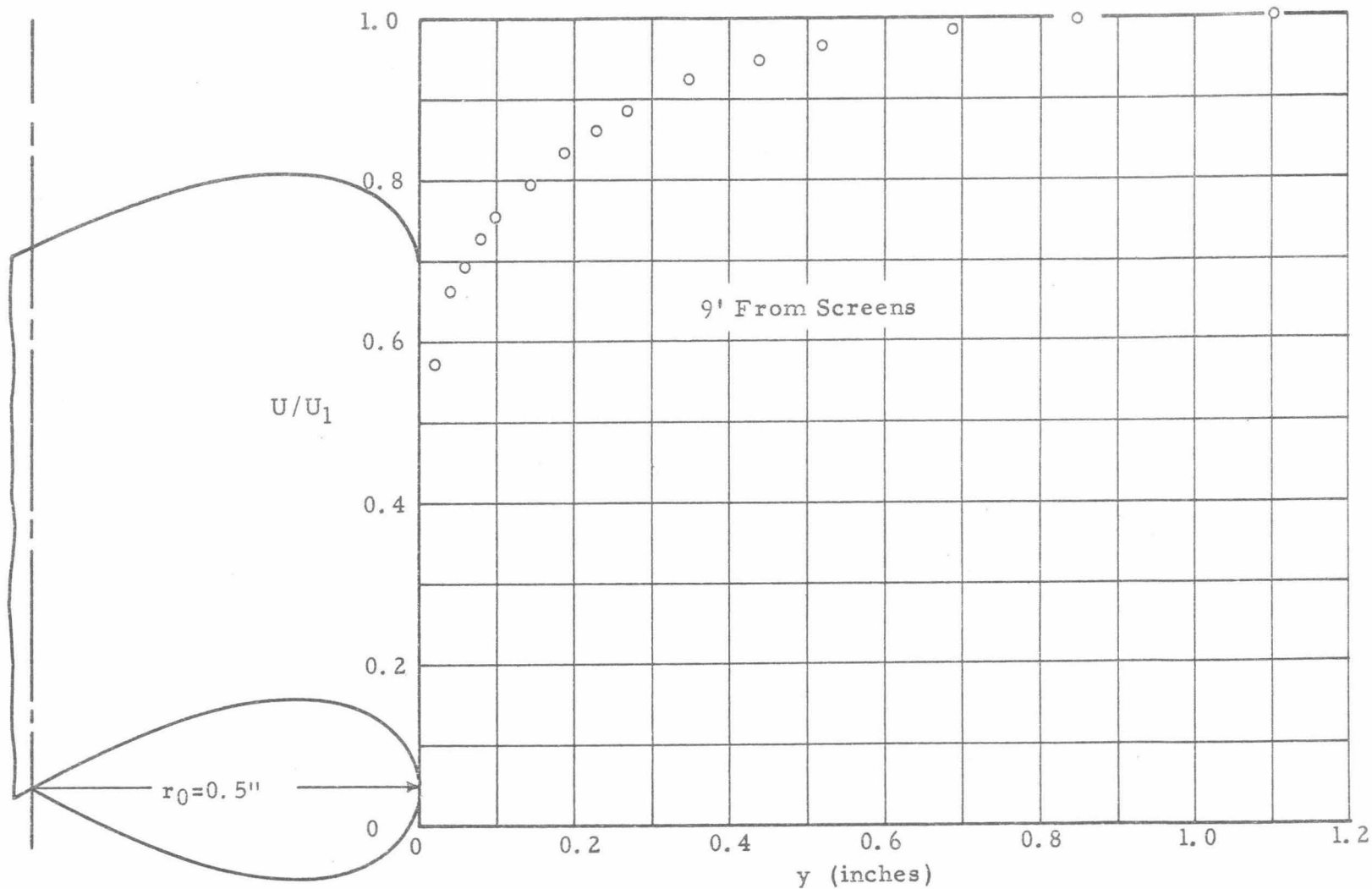
- T= General Radio Shielded Transformer
- L= Crescent Engineering "Transducer"
- D<sub>1</sub>, D<sub>2</sub>= 1N34A Sylvania Germanium Diodes
- C<sub>1</sub>, C<sub>2</sub>= 0.25 Microfarads
- R<sub>1</sub>, R<sub>2</sub>= 2000 Ohms
- R<sub>3</sub>= 14000 Ohms
- R<sub>4</sub>= 300 Ohms
- R<sub>5</sub>= 200 Ohm Ten Turn Helipot
- R<sub>6</sub>= 500 Ohms

ELECTRIC CIRCUIT FOR THE SKIN FRICTION METER

FIGURE 7

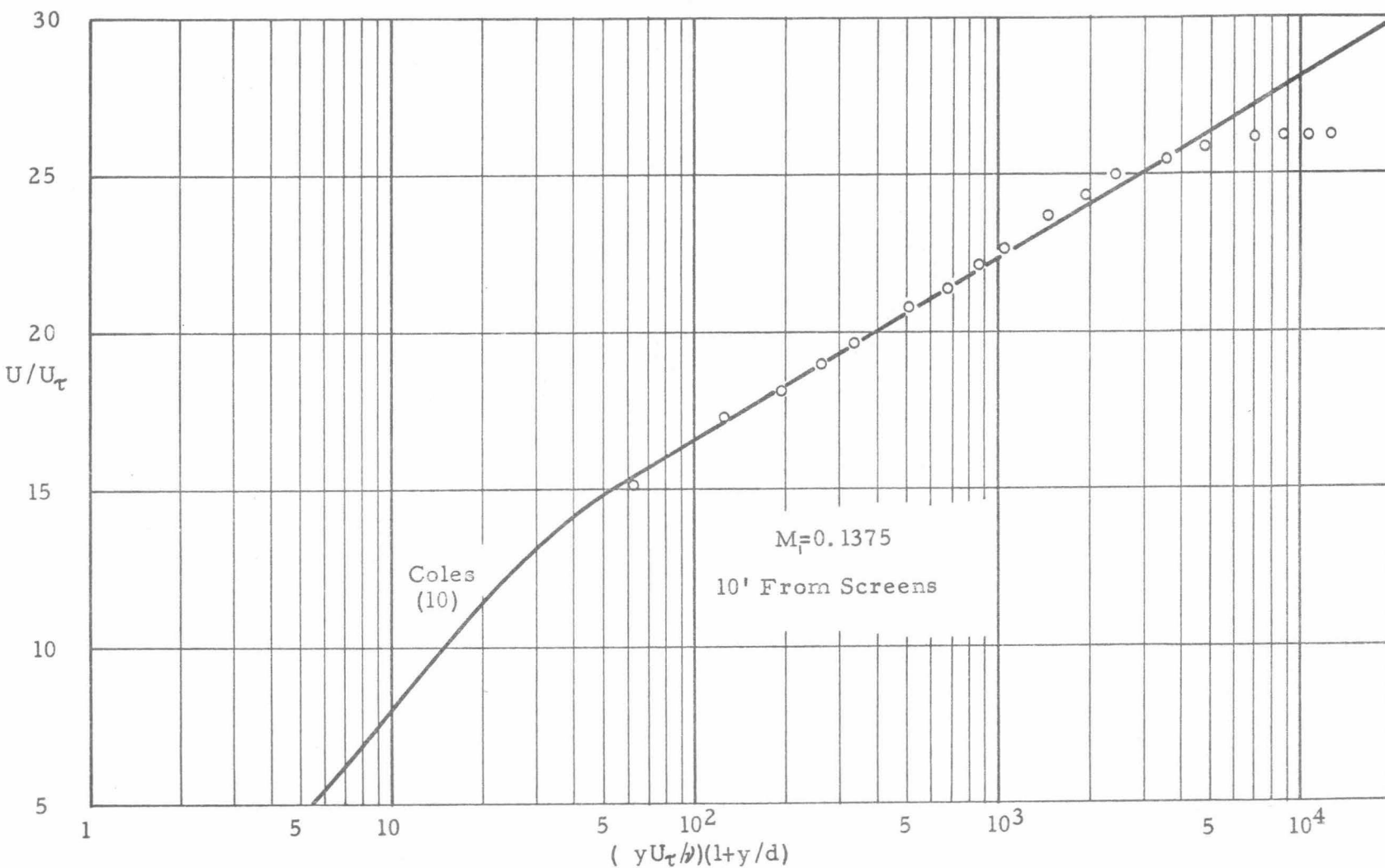


TYPICAL CALIBRATION OF THE SKIN FRICTION METER  
FIGURE 8



TURBULENT BOUNDARY LAYER PROFILE WITH AXIAL FLOW ON A 1 INCH DIAMETER CYLINDER  
IN THE MERRILL WIND TUNNEL

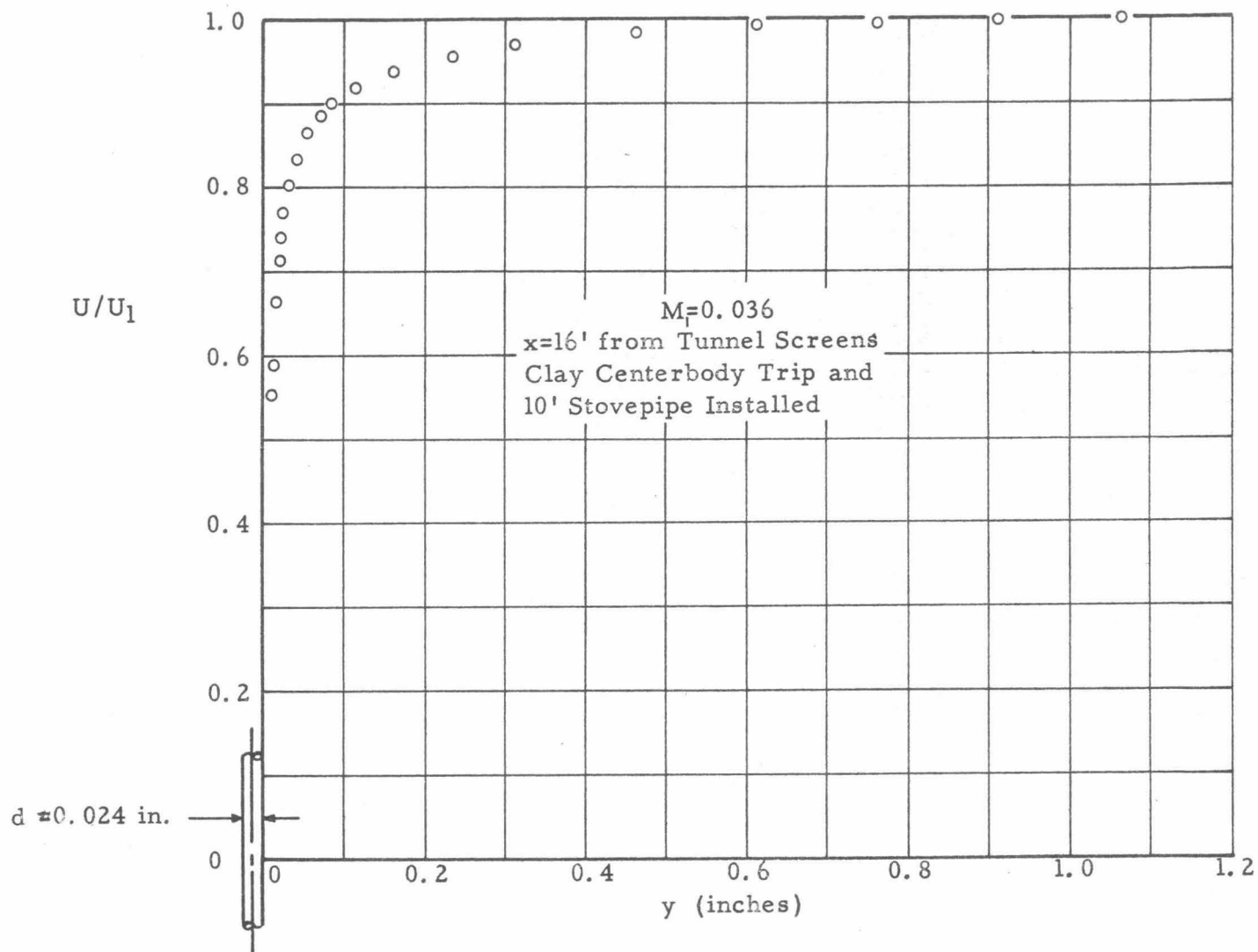
FIGURE 9a



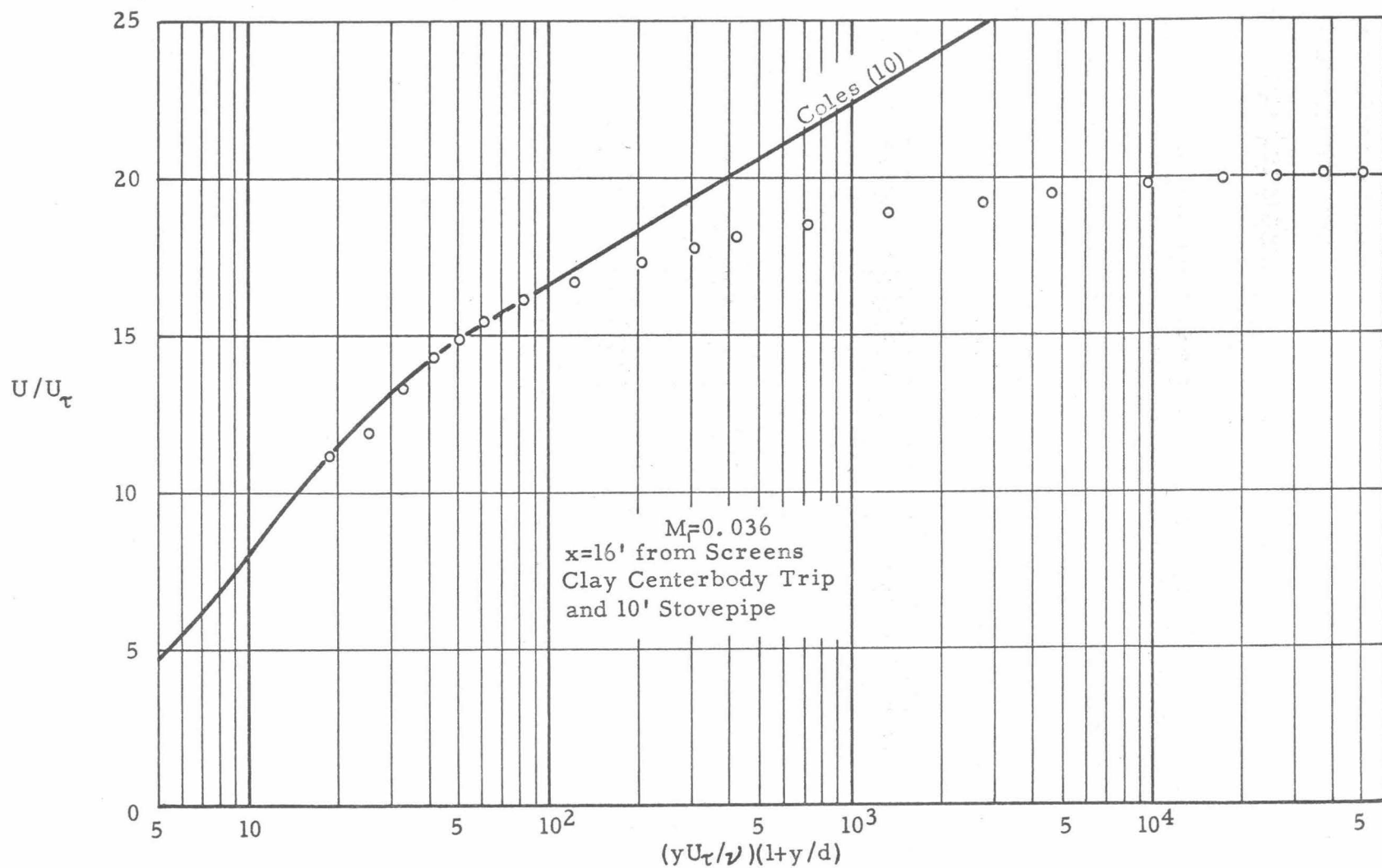
TURBULENT BOUNDARY LAYER PROFILE WITH AXIAL FLOW ON A 1 INCH DIAMETER CYLINDER  
IN THE MERRILL WIND TUNNEL

FIGURE 9b



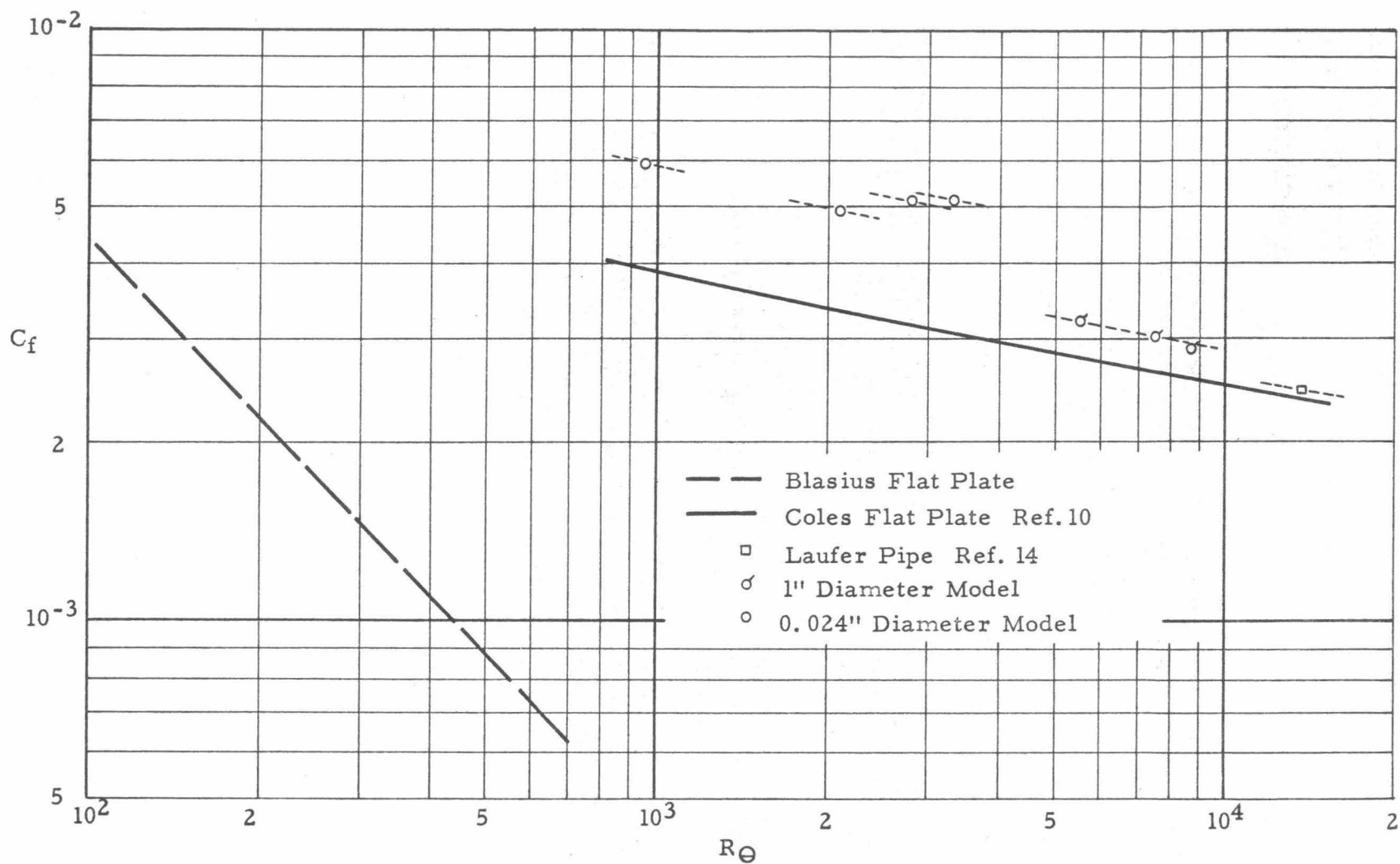


TURBULENT BOUNDARY LAYER PROFILE WITH AXIAL FLOW ON A 0.024 INCH DIAM. CYLINDER  
 IN THE LOW TURBULENCE WIND TUNNEL  
 FIGURE 10a

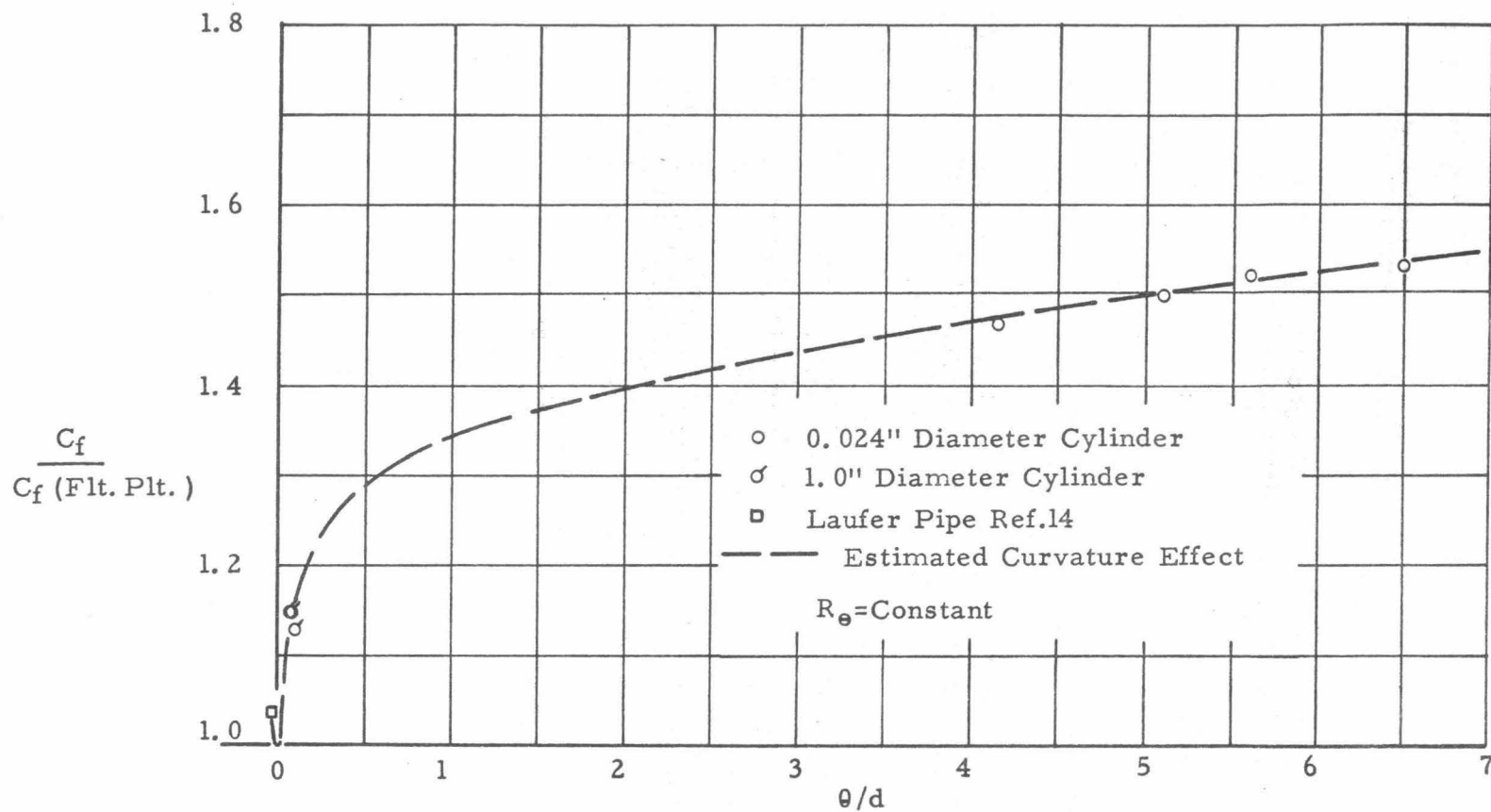


TURBULENT BOUNDARY LAYER PROFILE WITH AXIAL FLOW ON A 0.024 INCH DIAM. CYLINDER  
 IN THE LOW TURBULENCE WIND TUNNEL

FIGURE 10b

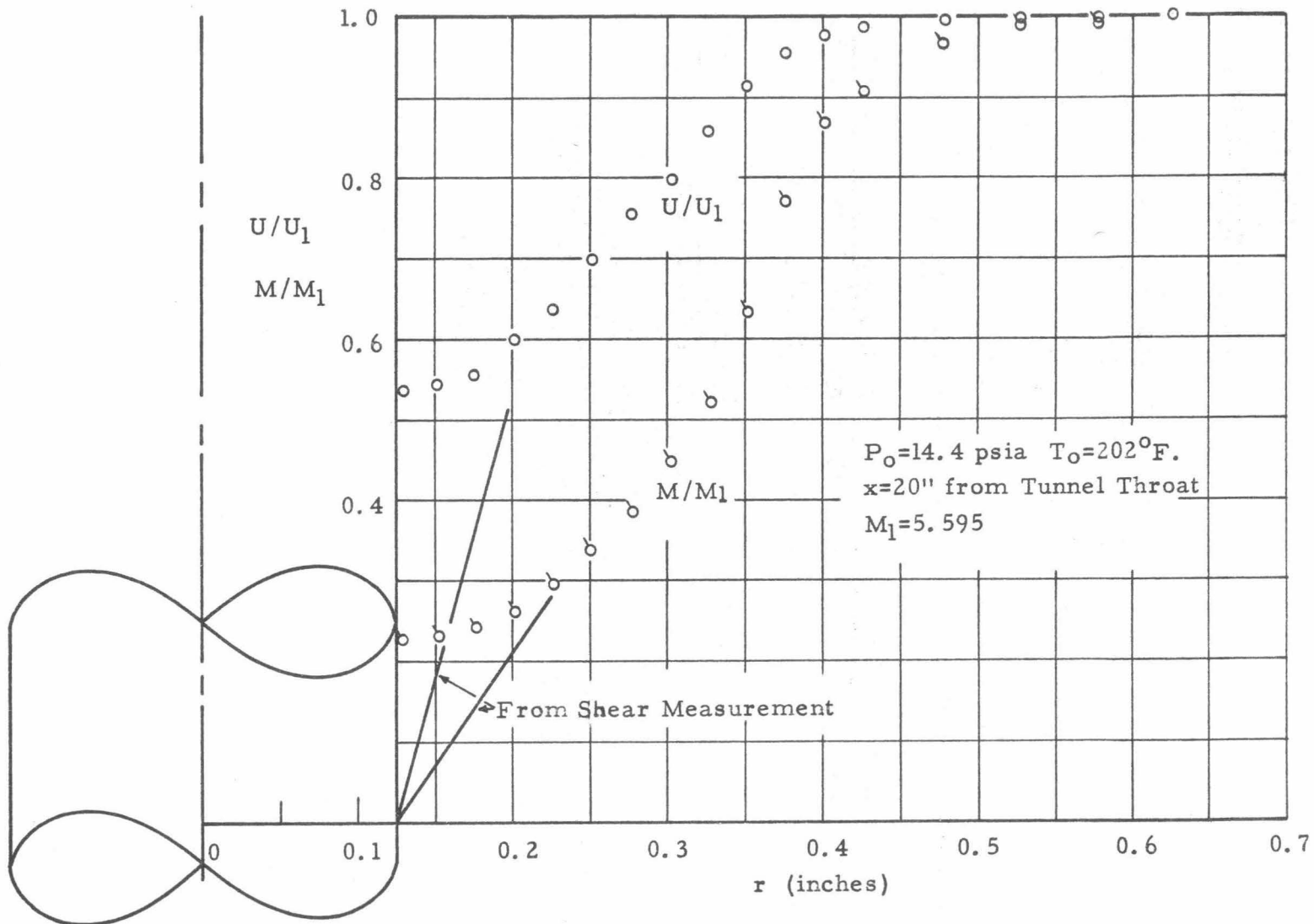


SUBSONIC TURBULENT BOUNDARY LAYER ESTIMATED SKIN FRICTION  
FIGURE 11

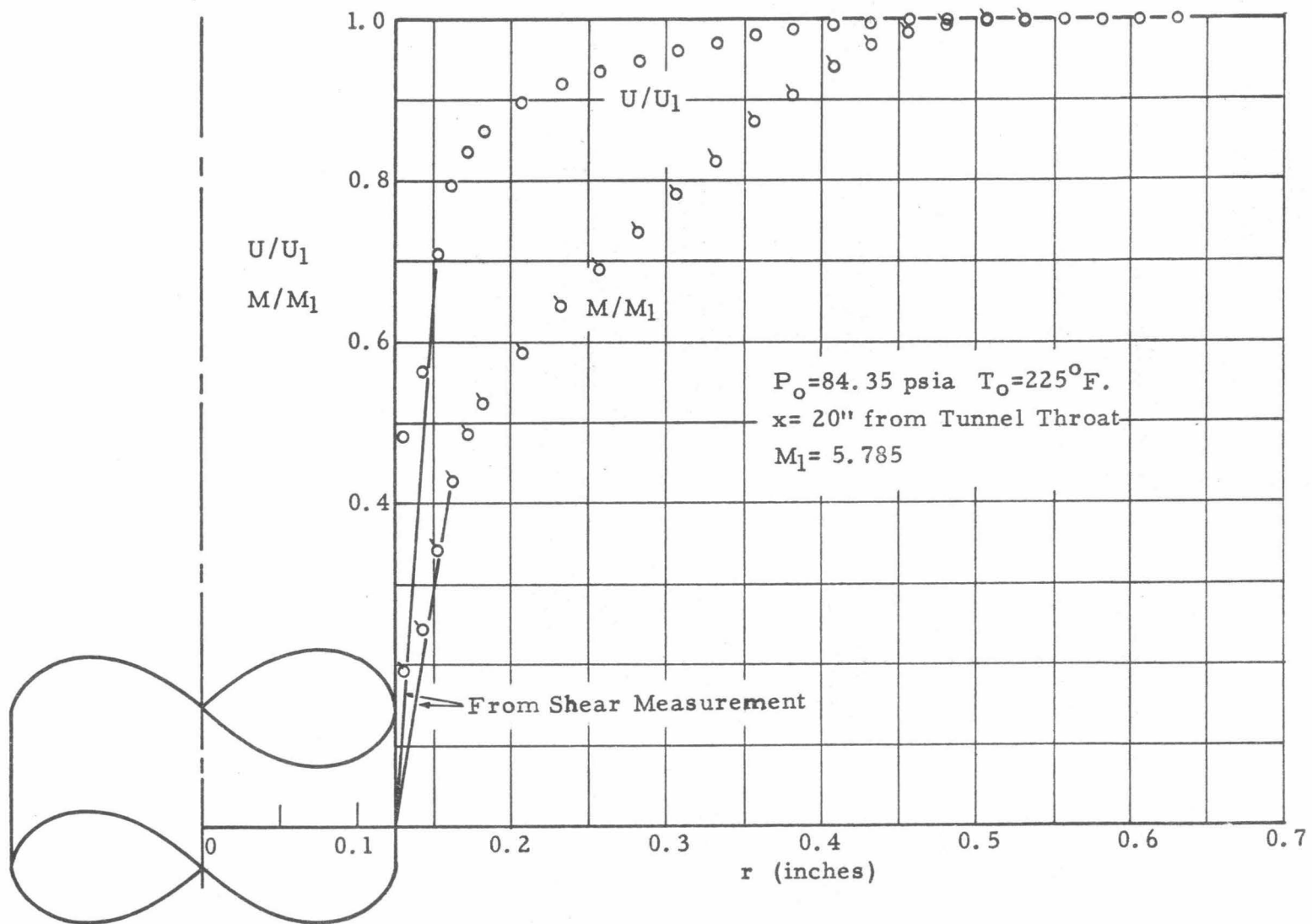


RATIO OF TURBULENT SKIN FRICTION ON A CYLINDER TO THAT ON A FLAT PLATE  
AT SUBSONIC SPEEDS

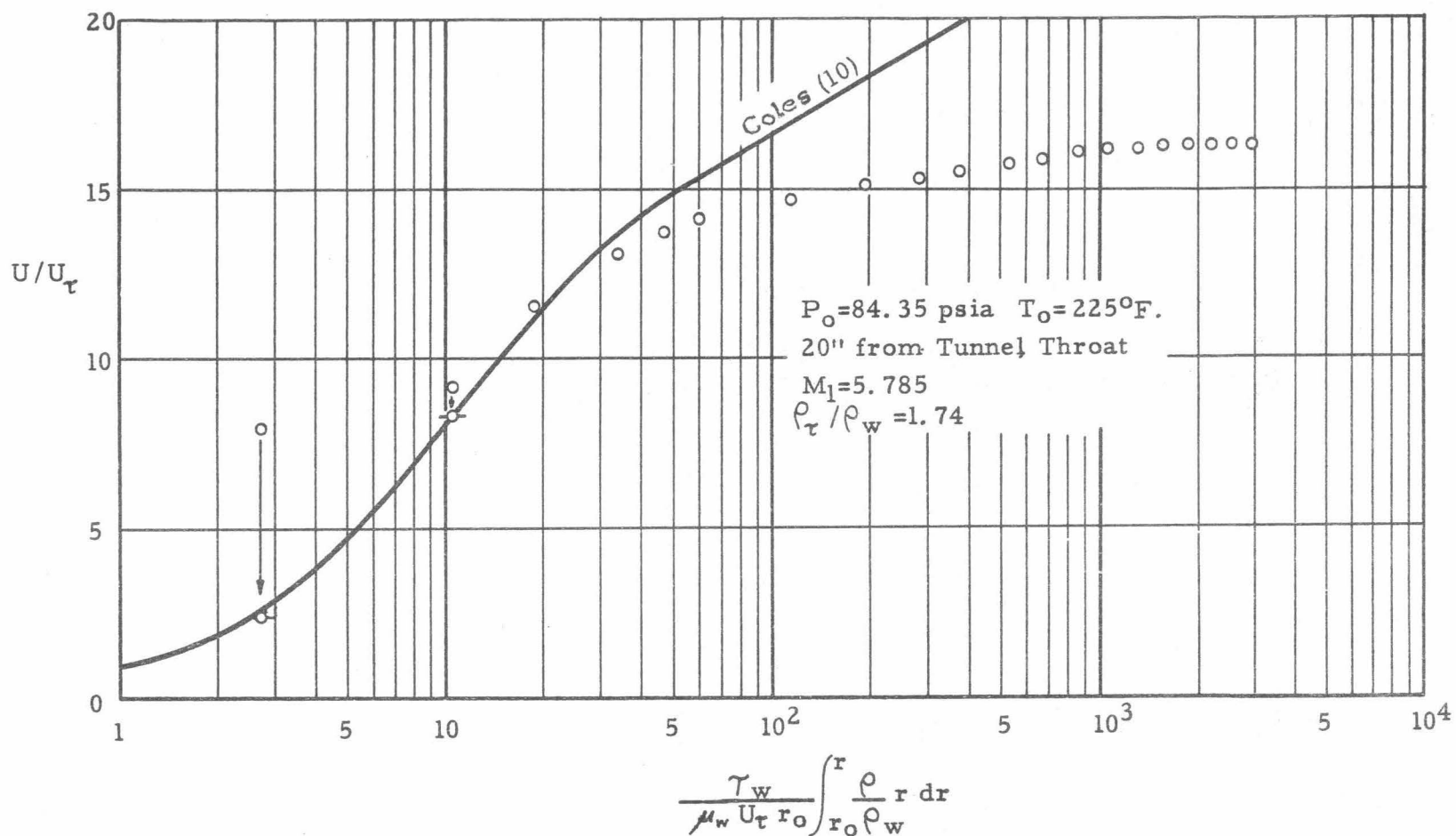
FIGURE 12



LAMINAR BOUNDARY LAYER PROFILE WITH AXIAL FLOW ON A 0.250 INCH DIAM. CYLINDER  
 IN THE 5x5 INCH HYPERSONIC WIND TUNNEL  
 FIGURE 13

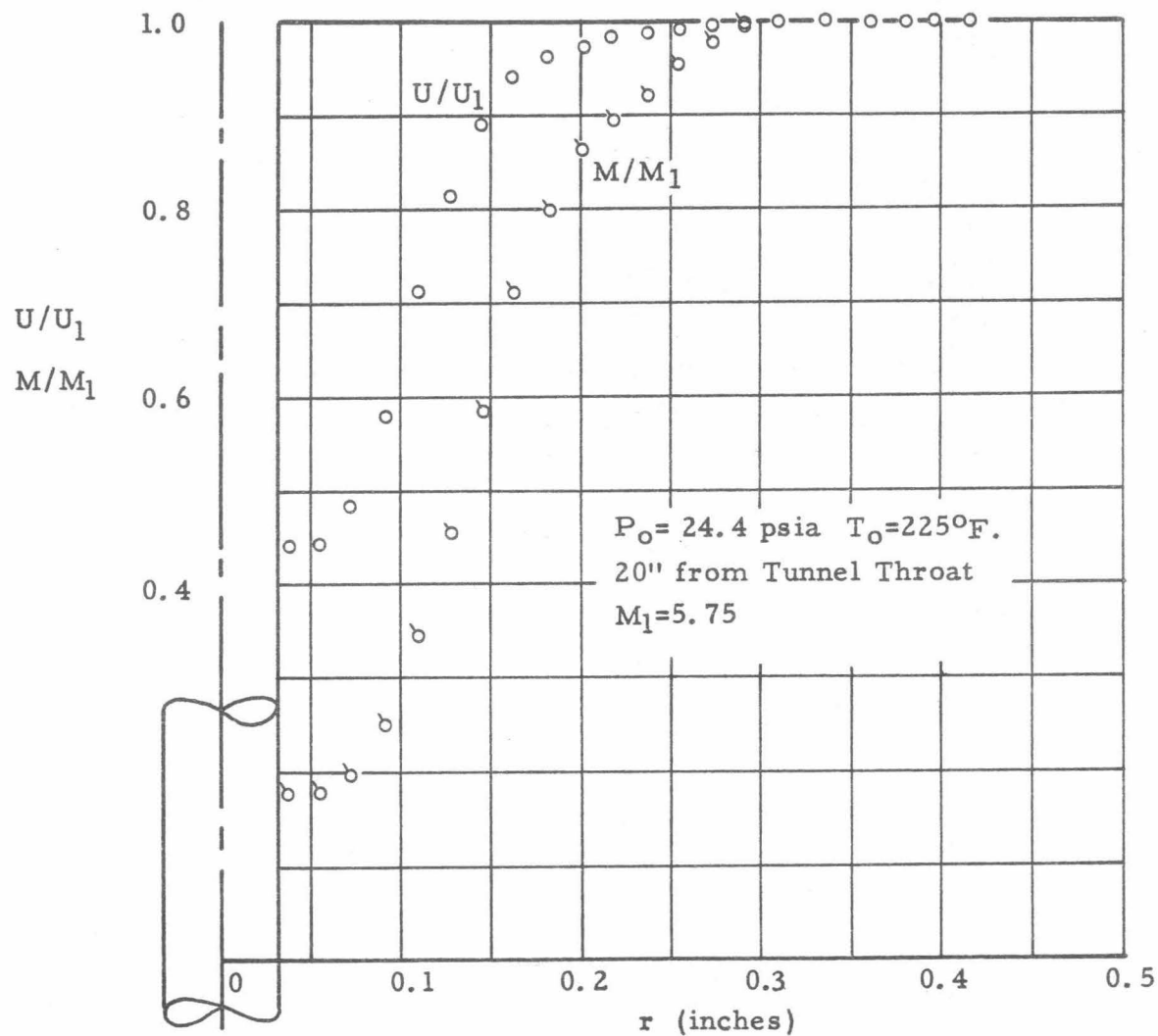


TURBULENT BOUNDARY LAYER PROFILE WITH AXIAL FLOW ON A 0.250 INCH DIAM. CYLINDER  
 IN THE 5x5 INCH HYPERSONIC WIND TUNNEL  
 FIGURE 14a



TURBULENT BOUNDARY LAYER PROFILE WITH AXIAL FLOW ON A 0.250 INCH DIAM. CYLINDER  
IN THE 5x5 INCH HYPERSONIC WIND TUNNEL

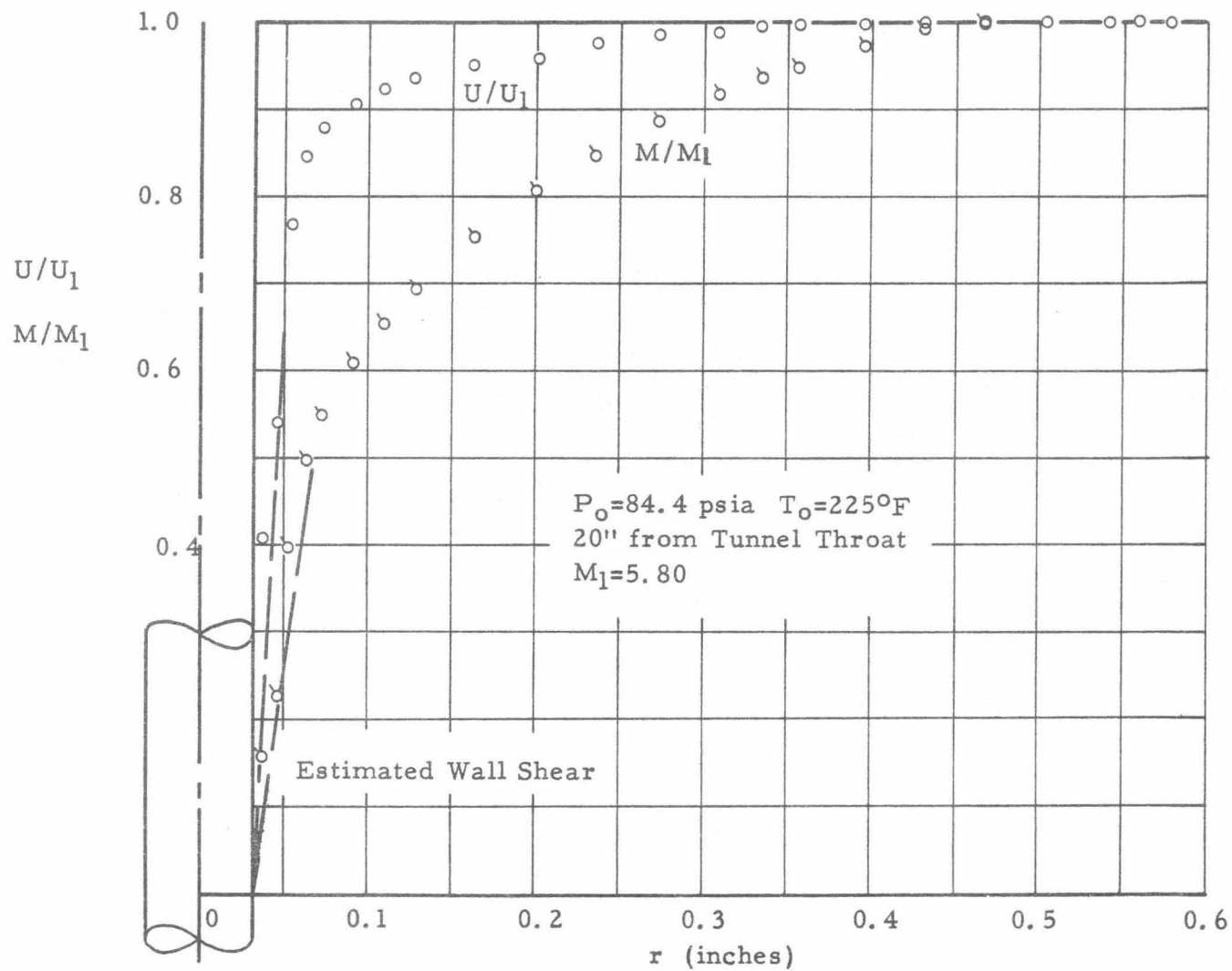
FIGURE 14b



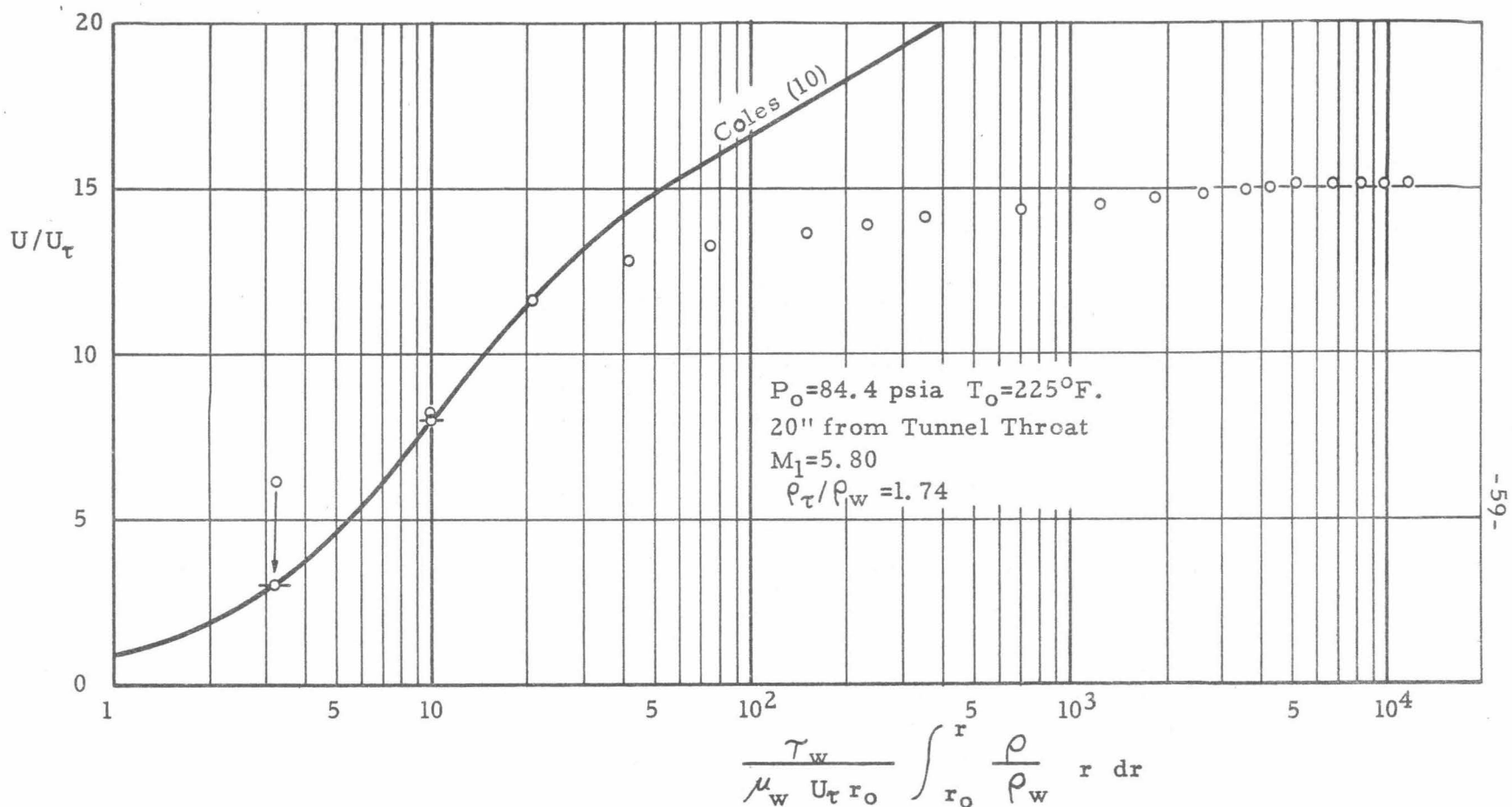
LAMINAR BOUNDARY LAYER PROFILE WITH AXIAL FLOW ON A 0.064 INCH DIAM. CYLINDER  
 IN THE 5x5 INCH HYPERSONIC WIND TUNNEL

FIGURE 15





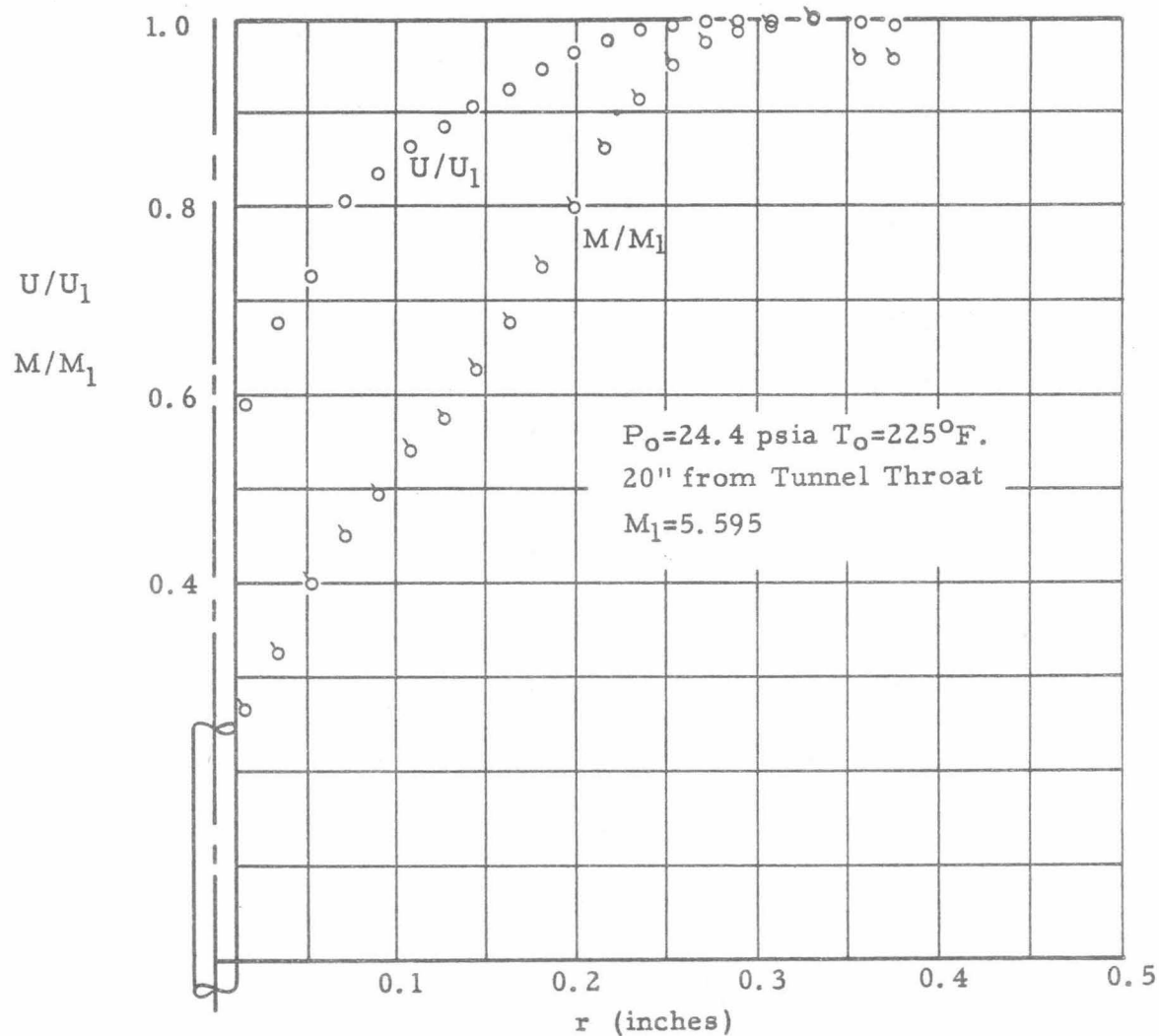
TURBULENT BOUNDARY LAYER PROFILE WITH AXIAL FLOW ON A 0.064 INCH DIAM. CYLINDER  
 IN THE 5x5 INCH HYPERSONIC WIND TUNNEL  
 FIGURE 16a



-59-

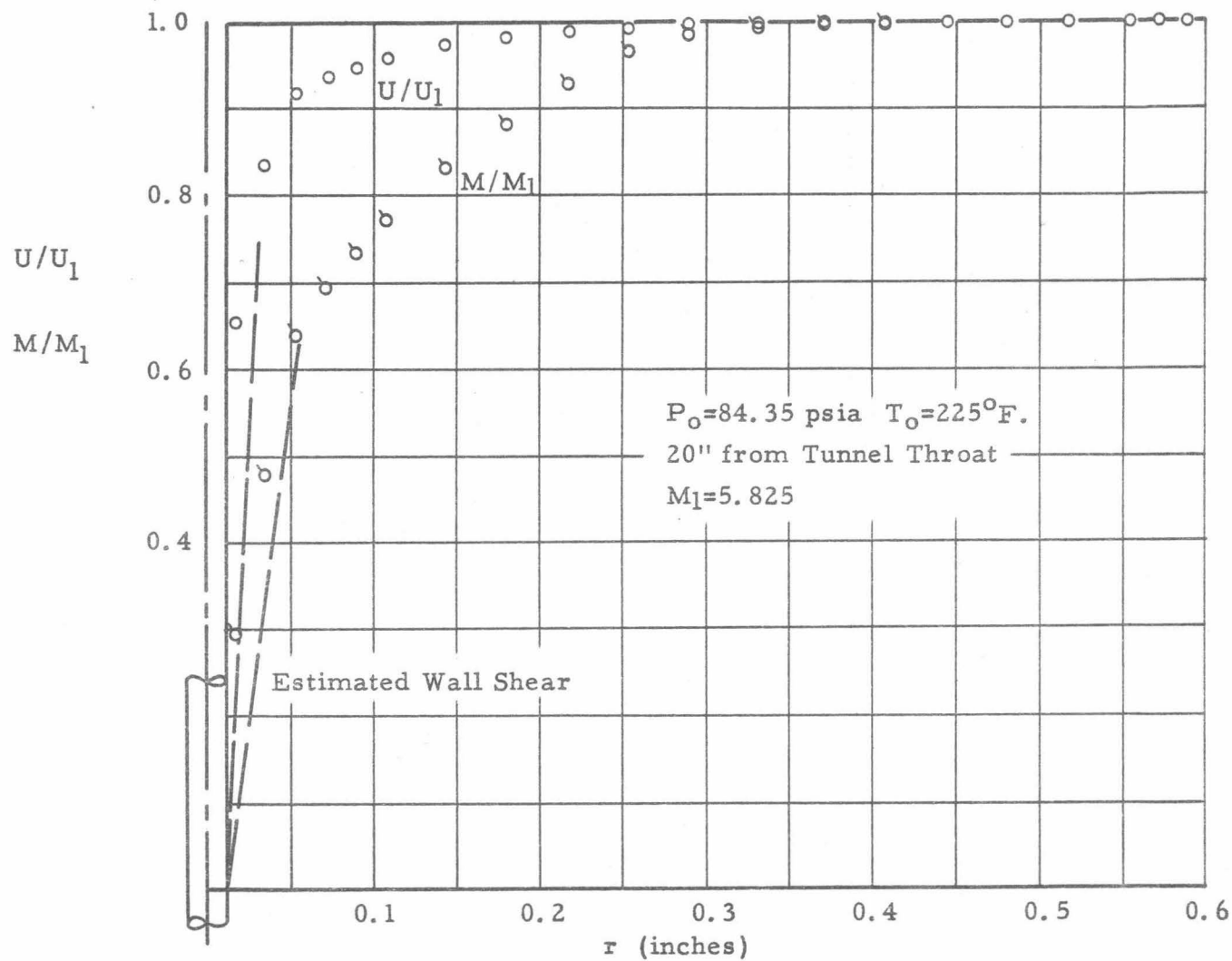
TURBULENT BOUNDARY LAYER PROFILE WITH AXIAL FLOW ON A 0.064 INCH DIAM. CYLINDER  
 IN THE 5x5 INCH HYPERSONIC WIND TUNNEL

FIGURE 16b

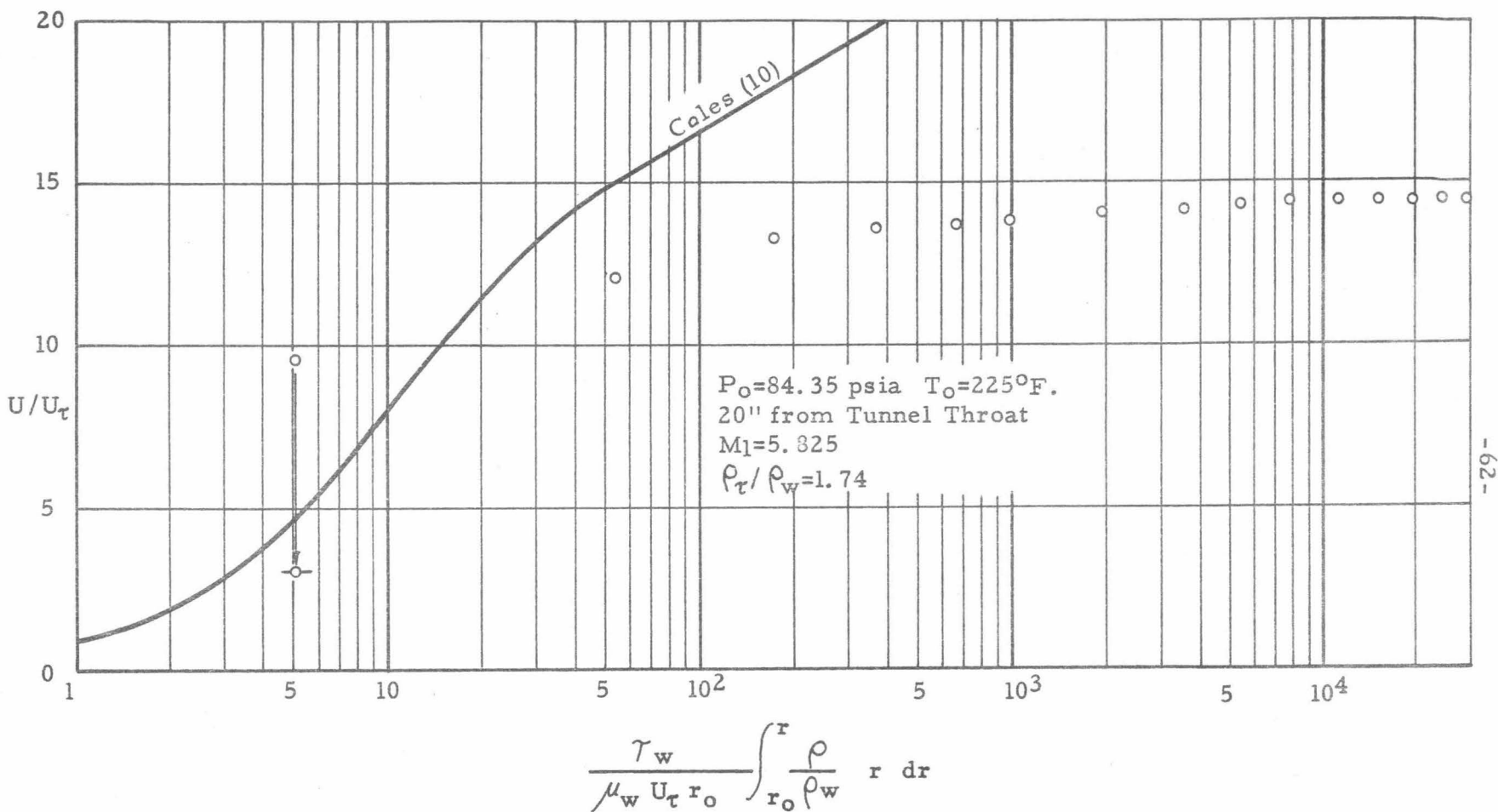


LAMINAR BOUNDARY LAYER PROFILE WITH AXIAL FLOW ON A 0.024 INCH DIAM. CYLINDER  
 IN THE 5x5 INCH HYPERSONIC WIND TUNNEL

FIGURE 17

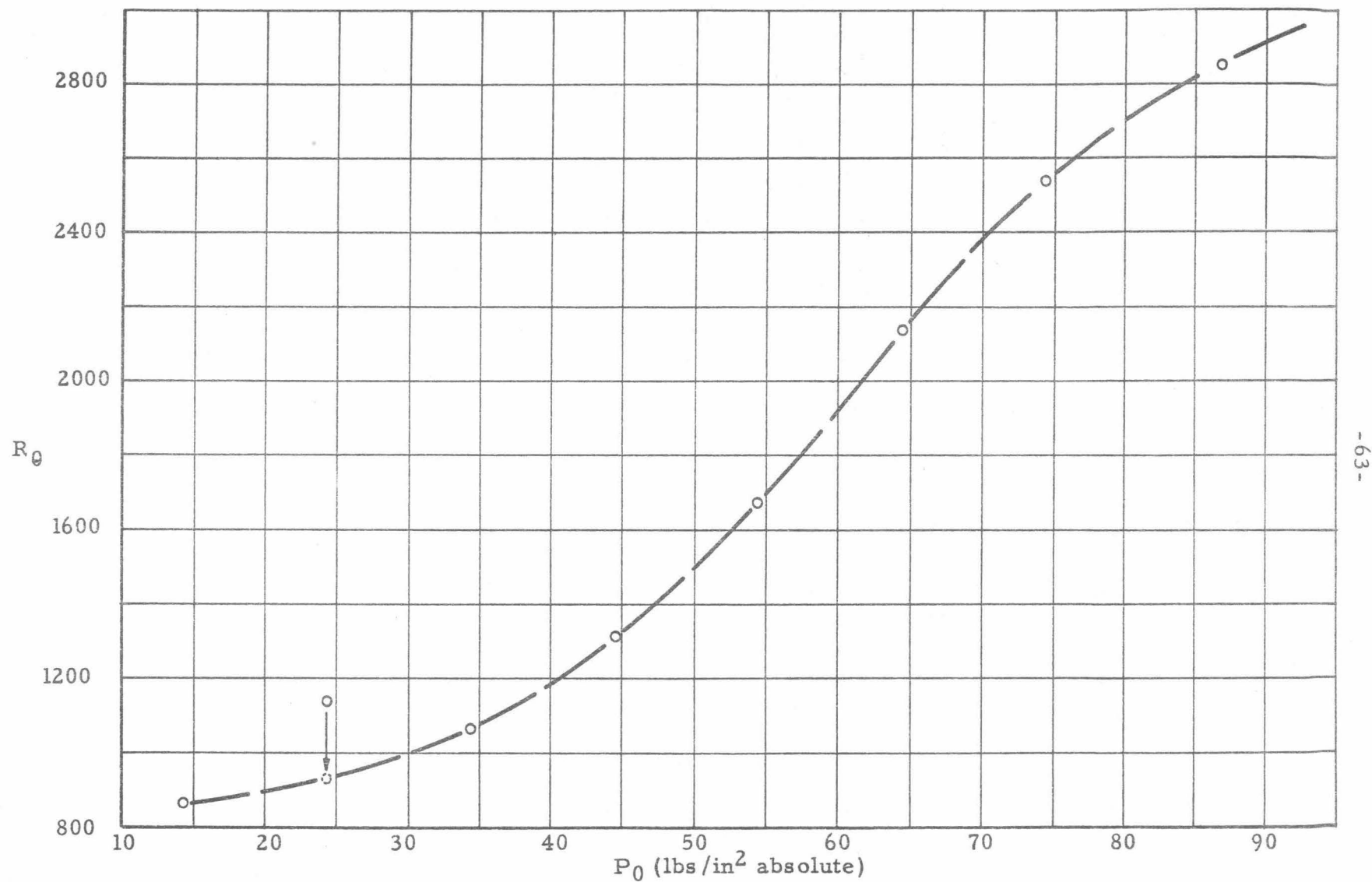


TURBULENT BOUNDARY LAYER PROFILE WITH AXIAL FLOW ON A 0.024 INCH DIAM. CYLINDER  
 IN THE 5x5 INCH HYPERSONIC WIND TUNNEL  
 FIGURE 18a

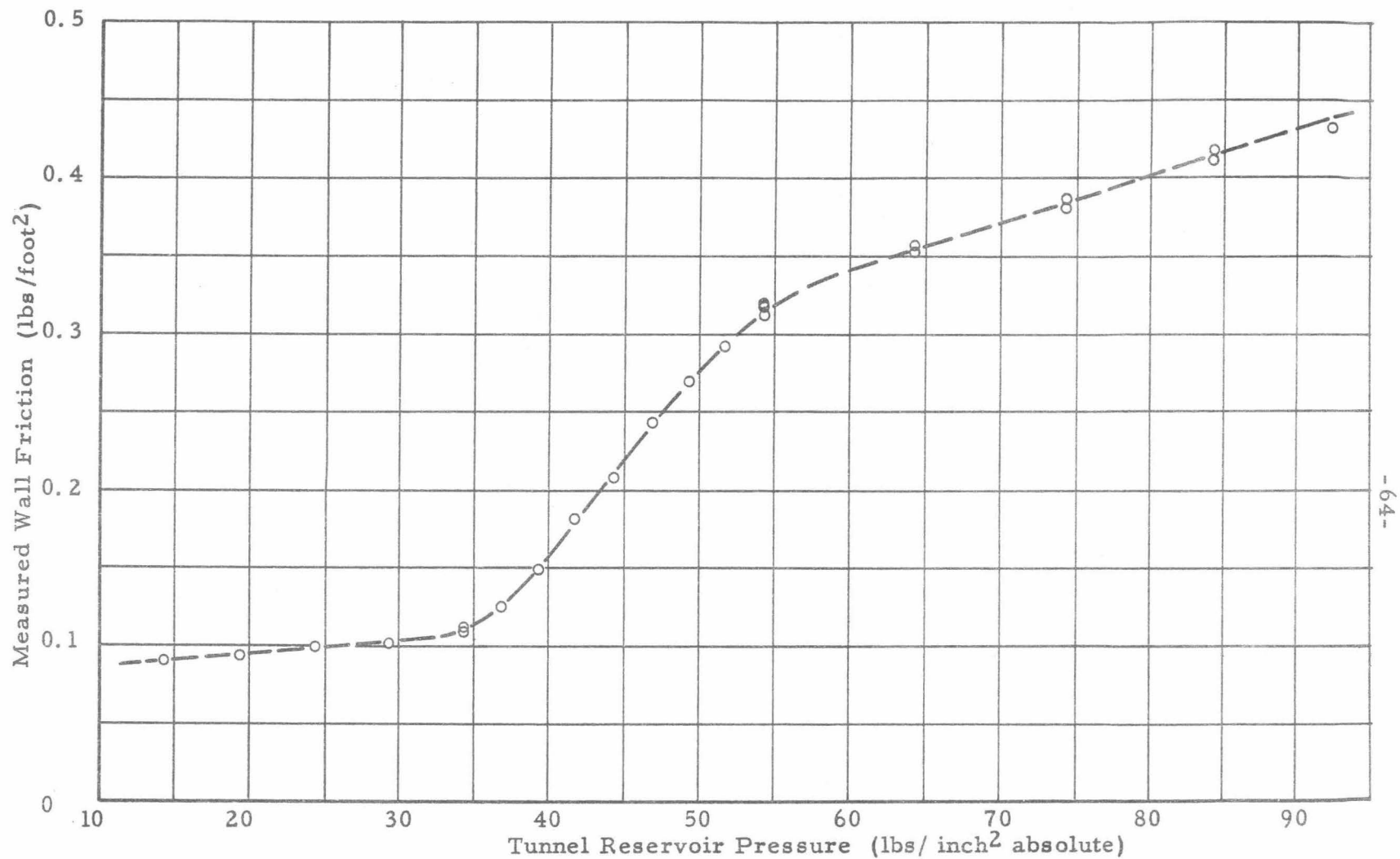


TURBULENT BOUNDARY LAYER PROFILE WITH AXIAL FLOW ON A 0.024 INCH DIAM. CYLINDER  
IN THE 5x5 INCH HYPERSONIC WIND TUNNEL

FIGURE 18b



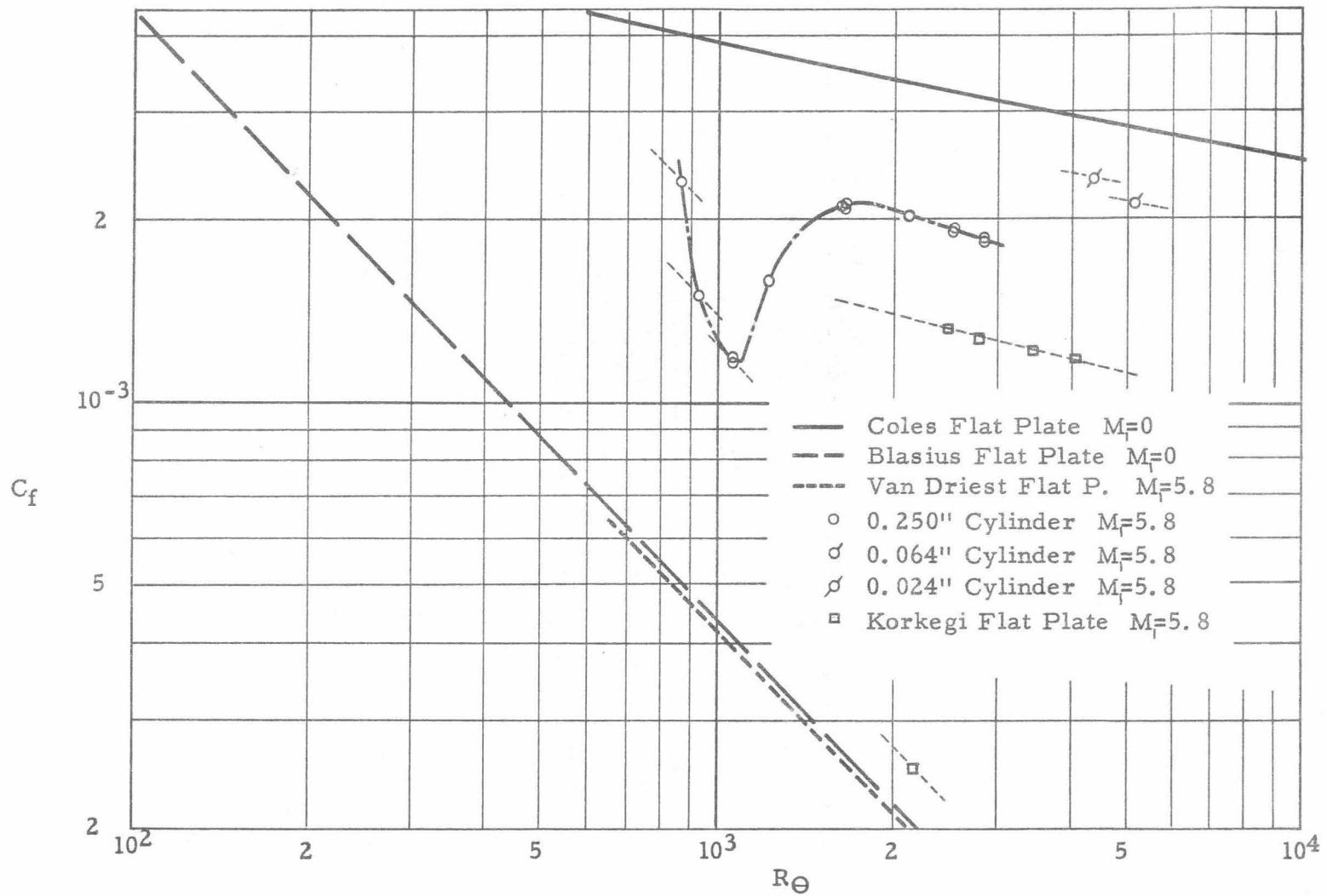
COMPUTED MOMENTUM THICKNESS REYNOLDS NUMBER ON THE 0.250 INCH SKIN FRICTION MODEL  
FIGURE 19



-64-

MEASURED SKIN FRICTION ON THE 0.250 INCH MODEL VERSES TUNNEL RESERVOIR PRESSURE

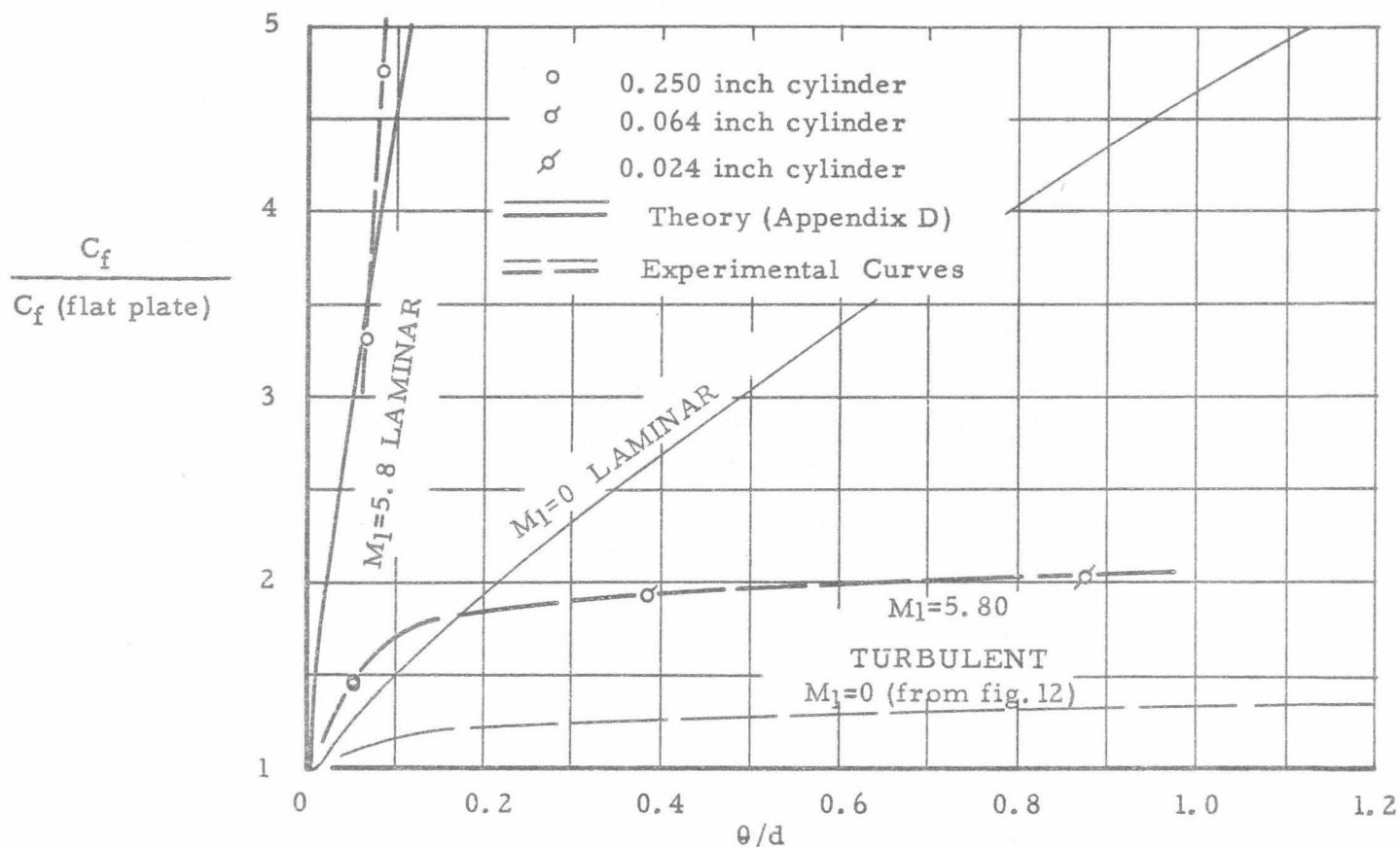
FIGURE 20



HYPERSONIC LAMINAR AND TURBULENT BOUNDARY LAYER SKIN FRICTION

FIGURE 21





RATIO OF SKIN FRICTION ON A CYLINDER TO THAT ON A FLAT PLATE AT  $M=0$  and  $M=5.8$   
AT CONSTANT  $R_\theta$

FIGURE 22

March 15, 1957

GUGGENHEIM AERONAUTICAL LABORATORY  
CALIFORNIA INSTITUTE OF TECHNOLOGY

HYPERSONIC RESEARCH PROJECT  
Contract No. DA-04-495-Ord-19

DISTRIBUTION LIST

U. S. Government Agencies

Los Angeles Ordnance District  
55 South Grand Avenue  
Pasadena 2, California  
Attention: Mr. E. L. Stone  
2 copies

Los Angeles Ordnance District  
55 South Grand Avenue  
Pasadena 2, California  
Attention: ORDEV-00-  
Mr. Z. Typaldos

Chief of Ordnance  
Department of the Army  
ORDTB - Ballistic Section  
The Pentagon  
Washington 25, D. C.  
Attention: Mr. G. Stetson  
2 copies

Chief of Ordnance  
Department of the Army  
Washington 25, D. C.  
Attention: ORDTB  
For Transmittal To  
Department of Commerce  
Office of Technical Information

Chief of Ordnance  
Department of the Army  
Washington 25, D. C.  
Attention: ORDTB  
For Transmittal To  
Director of Intelligence  
Headquarters, USAF  
Washington 25, D. C.  
Attention: Foreign Liaison Branch  
For: The Aeronautical Research  
Institute of Sweden  
Ulvssunda 1, Sweden  
Attention: Mr. Georg Drougge

Chief of Ordnance  
Department of the Army  
Washington 25, D. C.  
Attention: ORDGU-SE  
For Transmittal To  
Canadian Joint Staff

Chief of Ordnance  
Department of the Army  
Washington 25, D. C.  
Attention: ORDGU-SE  
For Transmittal To  
Foreign Relations Section  
For Australian Joint Services Mission

Office of Ordnance Research  
Box CM, Duke Station  
Durham, North Carolina  
10 copies

Ordnance Aerophysics Laboratory  
Daingerfield, Texas  
Attention: Mr. R. J. Valluz

Commanding General  
Army Ballistics Missile Agency  
Huntsville, Alabama  
Attention: ORDAB-1P  
2 copies

Commanding General  
Army Ballistics Missile Agency  
Huntsville, Alabama  
Attention: ORDAB-DA  
Mr. T. G. Reed  
3 copies

Commanding General  
Redstone Arsenal  
Huntsville, Alabama  
Attention: Technical Library

Commanding General  
Redstone Arsenal  
Huntsville, Alabama  
Attention: Dr. E. Geissler

Deputy Chief of Staff for Logistics  
U. S. Army  
Research and Development Division  
Washington, D. C.  
Attention: Research Branch

Exterior Ballistic Laboratories  
Aberdeen Proving Ground  
Maryland  
Attention: Mr. C. L. Poor

Ballistic Research Laboratories  
Aberdeen Proving Ground  
Maryland  
Attention: Dr. Joseph Sternberg

Commanding General  
White Sands Proving Ground  
Las Cruces, New Mexico

Western Division  
Headquarters  
Office of Scientific Research  
Air Research and Development  
Command  
P. O. Box 2035  
Pasadena 2, California  
Attention: Dr. M. Alperin

Commanding General  
Headquarters  
Office of Scientific Research  
Air Research and Development  
Command  
P. O. Box 1395  
Baltimore 3, Maryland  
Attention: RDTRRF

Mechanics Division  
Office of Scientific Research  
Air Research and Development  
Command  
P. O. Box 1395  
Baltimore 3, Maryland

Air Force Armament Center  
Air Research and Development  
Command  
Eglin Air Force Base  
Florida  
Attention: Technical Library

Air Research and Development  
Command  
European Office  
Shell Building  
60 Rue Rabenstein  
Brussels, Belgium  
Attention: Col. Lee Gossick, Chief  
5 copies

Commander  
Wright Air Development Center  
Wright-Patterson Air Force Base  
Ohio  
Attention: WCLSR

Commander  
Wright Air Development Center  
Wright-Patterson Air Force Base  
Ohio  
Attention: WCLSW

Commander  
Wright Air Development Center  
Wright-Patterson Air Force Base  
Ohio  
Attention: WCLSW, Mr. P. Antonatos

Commander  
Wright Air Development Center  
Wright-Patterson Air Force Base  
Ohio  
Attention: Dr. H. K. Doetsch

Director of Research and Development  
DCS/D  
Headquarters  
USAF  
Washington 25, D. C.  
Attention: AFDRD-RE

Commander  
Western Development Division  
P. O. Box 262  
Inglewood, California

Commander  
Western Development Division  
5760 Arbor Vitae Street  
Los Angeles, California  
Attention: Brig. Gen. B. A. Schriever

Commander  
Arnold Engineering Development Center  
Tullahoma, Tennessee  
Attention: AEORL

Commander  
Arnold Engineering Development Center  
Tullahoma, Tennessee  
Attention: Col. F. H. Richardson

Air University Library  
Maxwell Air Force Base  
Alabama

Homomann Air Force Base  
Alamogordo, New Mexico  
Attention: Dr. G. Eber

U. S. Naval Ordnance Laboratory  
White Oak  
Silver Spring, Maryland  
Attention: Dr. H. Kurzweg

U. S. Naval Ordnance Laboratory  
White Oak  
Silver Spring 19, Maryland  
Attention: Dr. R. K. Lobb

U. S. Naval Ordnance Laboratory  
White Oak  
Silver Spring 19, Maryland  
Attention: Dr. Z. I. Slawsky

U. S. Naval Ordnance Test Station  
China Lake  
Inyokern, California  
Attention: Mr. Howard R. Kelly, Head  
Aerodynamics Branch,  
Code 5032

Navy Department  
Bureau of Ordnance  
Technical Library  
Washington 25, D. C.  
Attention: Ad-3

Director  
Naval Research Laboratory  
Washington 25, D. C.

Office of Naval Research  
Department of the Navy  
Washington 25, D. C.

Commanding Officer  
Office of Naval Research  
Branch Office  
Navy, 100  
FPO  
New York, N. Y.  
2 copies

Commander  
U. S. Naval Proving Ground  
Dahlgren, Virginia

Bureau of Aeronautics  
Department of the Navy  
Room 2 w 75  
Washington 25, D. C.  
Attention: Mr. F. A. Loudon

U. S. Naval Air Missile Test Center  
Point Mugu, California  
Attention: Mr. J. H. Carrington,  
Chief Engineer

Armed Services Technical  
Information Agency  
Document Service Center  
Knott Building  
Dayton 2, Ohio  
Attention: DSC-SD22  
5 copies

National Bureau of Standards  
Department of Commerce  
Washington 25, D. C.  
Attention: Dr. G. B. Schubauer

National Advisory Committee  
for Aeronautics  
1512 H Street, N. W.  
Washington 25, D. C.  
Attention: Dr. H. L. Dryden, Director

National Advisory Committee  
for Aeronautics  
Ames Aeronautical Laboratory  
Moffett Field, California  
Attention: Mr. H. Julian Allen

National Advisory Committee  
for Aeronautics  
Ames Aeronautical Laboratory  
Moffett Field, California  
Attention: Dr. D. Chapman

National Advisory Committee  
for Aeronautics  
Ames Aeronautical Laboratory  
Moffett Field, California  
Attention: Dr. A. C. Charters

National Advisory Committee  
for Aeronautics  
Ames Aeronautical Laboratory  
Moffett Field, California  
Attention: Mr. A. J. Eggers

National Advisory Committee  
for Aeronautics  
Ames Aeronautical Laboratory  
Moffett Field, California  
Attention: Dr. M. K. Rubesin

National Advisory Committee  
for Aeronautics  
Ames Aeronautical Laboratory  
Moffett Field, California  
Attention: Mr. J. R. Stalder

National Advisory Committee  
for Aeronautics  
Langley Aeronautical Laboratory  
Langley Field, Virginia  
Attention: Mr. M. Bertram

National Advisory Committee  
for Aeronautics  
Langley Aeronautical Laboratory  
Langley Field, Virginia  
Attention: Dr. A. Buseman

National Advisory Committee  
for Aeronautics  
Langley Aeronautical Laboratory  
Langley Field, Virginia  
Attention: Mr. C. McLellan

National Advisory Committee  
for Aeronautics  
Langley Aeronautical Laboratory  
Langley Field, Virginia  
Attention: Mr. John Stack

National Advisory Committee  
for Aeronautics  
Lewis Flight Propulsion Laboratory  
Cleveland Municipal Airport  
Cleveland 11, Ohio  
Attention: Dr. J. C. Evvard

National Advisory Committee  
for Aeronautics  
Lewis Flight Propulsion Laboratory  
Cleveland Municipal Airport  
Cleveland 11, Ohio  
Attention: Dr. A. Silverstein

Technical Information Service  
P. O. Box 62  
Oak Ridge, Tennessee

### Universities and Non-Profit Organizations

Brown University  
Graduate Division of Applied Mathematics  
Providence 12, Rhode Island  
Attention: Professor W. Prager

Brown University  
Graduate Division of Applied Mathematics  
Providence 12, Rhode Island  
Attention: Dr. R. Probststein

University of California  
Low Pressures Research  
Institute of Engineering Research  
Engineering Field Station  
1301 South 46th Street  
Richmond, California  
Attention: Professor S. A. Schaaf

University of California at Los Angeles  
Department of Engineering  
Los Angeles 24, California  
Attention: Dr. L. M. K. Boelter

Case Institute of Technology  
Cleveland, Ohio  
Attention: Dr. G. Kuerti

Catholic University of America  
Department of Physics  
Washington 17, D. C.  
Attention: Professor K. F. Herzfeld

Cornell Aeronautical Laboratory  
Buffalo, New York  
Attention: Dr. A. Flax

Cornell Aeronautical Laboratory  
Buffalo, New York  
Attention: Dr. Ira G. Ross, Director

Cornell University  
Graduate School of Aeronautical Engineering  
Ithaca, New York  
Attention: Dr. W. R. Sears

Harvard University  
Department of Applied Physics and  
Engineering Science  
Cambridge 38, Massachusetts  
Attention: Dr. A. Bryson

Harvard University  
Department of Applied Physics and  
Engineering Science  
Cambridge 38, Massachusetts  
Attention: Dr. H. W. Emmons

University of Illinois  
Department of Aeronautical Engineering  
Urbana, Illinois  
Attention: Professor C. H. Fletcher

The Johns Hopkins University  
Applied Physics Laboratory  
8621 Georgia Avenue  
Silver Spring, Maryland  
Attention: Dr. E. A. Bonney

The Johns Hopkins University  
Applied Physics Laboratory  
8621 Georgia Avenue  
Silver Spring, Maryland  
Attention: Dr. F. N. Frenkiel

The Johns Hopkins University  
Applied Physics Laboratory  
8621 Georgia Avenue  
Silver Spring, Maryland  
Attention: Dr. F. K. Hill

The Johns Hopkins University  
Department of Aeronautical Engineering  
Baltimore 18, Maryland  
Attention: Dr. F. H. Clauser

The Johns Hopkins University  
Department of Aeronautical Engineering  
Baltimore 18, Maryland  
Attention: Dr. L. Kovasznay

The Johns Hopkins University  
Department of Mechanical Engineering  
Baltimore 18, Maryland  
Attention: Dr. S. Corrsin

Lehigh University  
Physics Department  
Bethlehem, Pennsylvania  
Attention: Dr. R. Emrich

University of Maryland  
Department of Aeronautical Engineering  
College Park, Maryland  
Attention: Dr. S. F. Shen

University of Maryland  
Institute of Fluid Dynamics and  
Applied Mathematics  
College Park, Maryland  
Attention: Director

University of Maryland  
Institute of Fluid Dynamics and  
Applied Mathematics  
College Park, Maryland  
Attention: Professor F. R. Hama

University of Maryland  
Institute of Fluid Dynamics and  
Applied Mathematics  
College Park, Maryland  
Attention: Dr. H. T. Yang

Massachusetts Institute of Technology  
Cambridge 39, Massachusetts  
Attention: Dr. A. H. Shapiro

Massachusetts Institute of Technology  
Department of Aeronautical Engineering  
Cambridge 39, Massachusetts  
Attention: Professor M. Finston

Massachusetts Institute of Technology  
Department of Aeronautical Engineering  
Cambridge 39, Massachusetts  
Attention: Professor J. R. Markham

Massachusetts Institute of Technology  
Department of Aeronautical Engineering  
Cambridge 39, Massachusetts  
Attention: Dr. G. Stever

University of Michigan  
Ann Arbor, Michigan  
Attention: Dr. H. P. Liepmann

University of Michigan  
Department of Aeronautical Engineering  
East Engineering Building  
Ann Arbor, Michigan  
Attention: Dr. Arnold Kuethe

University of Michigan  
Department of Aeronautical Engineering  
East Engineering Building  
Ann Arbor, Michigan  
Attention: Professor W. C. Nelson

University of Michigan  
Department of Physics  
Ann Arbor, Michigan  
Attention: Dr. O. Laporte

University of Minnesota  
Department of Aeronautical Engineering  
Minneapolis 14, Minnesota  
Attention: Professor J. D. Akerman

University of Minnesota  
Department of Aeronautical Engineering  
Minneapolis 14, Minnesota  
Attention: Dr. C. C. Chang

University of Minnesota  
Department of Aeronautical Engineering  
Minneapolis 14, Minnesota  
Attention: Dr. R. Hermann

University of Minnesota  
Department of Mechanical Engineering  
Division of Thermodynamics  
Minneapolis, Minnesota  
Attention: Dr. E. R. G. Eckert

New York University  
Department of Aeronautics  
University Heights  
New York 53, New York  
Attention: Dr. J. F. Ludloff

New York University  
Institute of Mathematics and Mechanics  
45 Fourth Street  
New York 53, New York  
Attention: Dr. R. W. Courant

North Carolina State College  
Department of Engineering  
Raleigh, North Carolina  
Attention: Professor R. M. Pinkerton

Ohio State University  
Aeronautical Engineering Department  
Columbus, Ohio  
Attention: Professor A. Tifford

Ohio State University  
Aeronautical Engineering Department  
Columbus, Ohio  
Attention: Professor G. L. von Eschen

Pennsylvania State College  
Department of Aeronautical Engineering  
State College, Pennsylvania  
Attention: Professor M. Lessen

Polytechnic Institute of Brooklyn  
Aerodynamic Laboratory  
527 Atlantic Avenue  
Freeport, New York  
Attention: Dr. A. Ferri

Polytechnic Institute of Brooklyn  
Aerodynamic Laboratory  
527 Atlantic Avenue  
Freeport, New York  
Attention: Dr. P. Libby

Princeton University  
Princeton, New Jersey  
Attention: Dr. Sin I. Cheng

Princeton University  
Forrestal Research Center  
Princeton, New Jersey  
Attention: Library

Princeton University  
Aeronautics Department  
Forrestal Research Center  
Princeton, New Jersey  
Attention: Professor S. Bogdonoff

Princeton University  
Aeronautics Department  
Forrestal Research Center  
Princeton, New Jersey  
Attention: Dr. L. Crocco

Princeton University  
Aeronautics Department  
Forrestal Research Center  
Princeton, New Jersey  
Attention: Professor Wallace Hayes

Princeton University  
Palmer Physical Laboratory  
Princeton, New Jersey  
Attention: Dr. W. Bleakney

Princeton University  
Palmer Physical Laboratory  
Princeton, New Jersey  
Attention: Dr. W. Griffith

Purdue University  
School of Aeronautical Engineering  
Lafayette, Indiana  
Attention: Librarian

Rensselaer Polytechnic Institute  
Aeronautics Department  
Troy, New York  
Attention: Dr. R. P. Harrington

Rensselaer Polytechnic Institute  
Aeronautics Department  
Troy, New York  
Attention: Dr. T. Y. Li

Rouss Physical Laboratory  
University of Virginia  
Charlottesville, Virginia  
Attention: Dr. J. W. Beams

Stanford University  
Department of Mechanical Engineering  
Palo Alto, California  
Attention: Dr. D. Bershader

University of Texas  
Defense Research Laboratory  
500 East 24th Street  
Austin, Texas  
Attention: Professor M. J. Thompson

University of Washington  
Department of Aeronautical Engineering  
Seattle 5, Washington  
Attention: Professor F. S. Eastman

University of Washington  
Department of Aeronautical Engineering  
Seattle 5, Washington  
Attention: Professor R. E. Street

University of Wisconsin  
Department of Chemistry  
Madison, Wisconsin  
Attention: Dr. J. O. Hirschfelder

Institute of the Aeronautical Sciences  
2 East 64th Street  
New York 21, New York  
Attention: Library

Midwest Research Institute  
4049 Pennsylvania  
Kansas City, Missouri  
Attention: Mr. M. Goland, Director  
for Engineering Sciences

National Science Foundation  
Washington 25, D. C.  
Attention: Dr. J. McMillan

National Science Foundation  
Washington 25, D. C.  
Attention: Dr. R. Seeger



# Industrial Companies

Aeronutronic Systems, Inc.  
1234 Air Way  
Glendale, California  
Attention: Dr. J. Charyk

Aeronutronic Systems, Inc.  
1234 Air Way  
Glendale, California  
Attention: Dr. L. Kovanau

Aerophysics Development Corp.  
P. O. Box 689  
Santa Barbara, California  
Attention: Librarian

ARO, Inc.  
P. O. Box 162  
Tullahoma, Tennessee  
Attention: Dr. B. Goethert

ARO, Inc.  
P. O. Box 162  
Tullahoma, Tennessee  
Attention: Mr. R. Smelt

AVCO Manufacturing Corp.  
2385 Revere Beach Parkway  
Everett 49, Massachusetts  
Attention: Library

AVCO Manufacturing Corp.  
2385 Revere Beach Parkway  
Everett 49, Massachusetts  
Attention: Dr. A. Kantrowitz

Bell Aircraft Corp.  
Aerodynamics Section  
P. O. Box 1  
Buffalo 5, New York  
Attention: Dr. Joel S. Isenberg

Bell Aircraft Corp.  
P. O. Box 1  
Buffalo 5, New York  
Attention: Mr. R. J. Woods

Boeing Airplane Company  
P. O. Box 3107  
Seattle 14, Washington  
Attention: Mr. G. Snyder

Chance Vought Aircraft, Inc.  
P. O. Box 5907  
Dallas, Texas  
Attention: Mr. J. R. Clark

Chance Vought Aircraft, Inc.  
P. O. Box 5907  
Dallas, Texas  
Attention: Dr. R. Wilson

CONVAIR  
Division of General Dynamics Corp.  
San Diego 12, California  
Attention: Mr. C. Bossart

CONVAIR  
Division of General Dynamics Corp.  
San Diego 12, California  
Attention: Mr. W. H. Dorrance  
Dept. 1-16

CONVAIR  
Division of General Dynamics Corp.  
San Diego 12, California  
Attention: Mr. W. B. Mitchell

CONVAIR  
Division of General Dynamics Corp.  
Fort Worth 1, Texas  
Attention: Mr. W. B. Fallis

CONVAIR  
Division of General Dynamics Corp.  
Fort Worth 1, Texas  
Attention: Mr. E. B. Maske

CONVAIR  
Division of General Dynamics Corp.  
Fort Worth 1, Texas  
Attention: Mr. W. G. McMullen

CONVAIR  
Division of General Dynamics Corp.  
Fort Worth 1, Texas  
Attention: Mr. R. H. Widmer

Cooperative Wind Tunnel  
950 South Raymond Avenue  
Pasadena, California  
Attention: Mr. F. Felberg

Cooperative Wind Tunnel  
950 South Raymond Avenue  
Pasadena, California  
Attention: Mr. E. I. Pritchard

Douglas Aircraft Company  
Santa Monica, California  
Attention: Mr. J. Gunkel

Douglas Aircraft Company  
Santa Monica, California  
Attention: Mr. Ellis Lapin

Douglas Aircraft Company  
Santa Monica, California  
Attention: Mr. H. Luskin

Douglas Aircraft Company  
Santa Monica, California  
Attention: Dr. W. B. Oswald

General Electric Company  
Research Laboratory  
Schenectady, New York  
Attention: Dr. H. T. Nagamatsu

General Electric Company  
Campbell Avenue Plant  
Schenectady, New York  
Attention: Mr. G. Metcalf

The Glenn L. Martin Company  
Baltimore 3, Maryland  
Attention: Mr. G. S. Trimble, Jr.

Grumman Aircraft Engineering Corp.  
Bethpage, New York  
Attention: Mr. C. Tilgner, Jr.

Hughes Aircraft Company  
Culver City, California  
Attention: Dr. A. E. Puckett

Lockheed Aircraft Corp.  
Missiles Division  
Van Nuys, California  
Attention: Library

Lockheed Missile Systems Division  
P. O. Box 504  
Sunnyvale, California  
Attention: Mr. Maurice Tucker

Lockheed Missile Systems Division  
P. O. Box 504  
Sunnyvale, California  
Attention: Dr. L. H. Wilson

Marquhardt Aircraft Company  
P. O. Box 2013 - South Annex  
Van Nuys, California  
Attention: Mr. E. T. Pitkin

McDonnell Aircraft Corp.  
Lambert-St. Louis Municipal Airport  
P. O. Box 516  
St. Louis 3, Missouri  
Attention: Mr. K. Perkins

North American Aviation, Inc.  
Aeronautical Laboratory  
Downey, California  
Attention: Dr. E. R. Van Driest

Northrop Aircraft, Inc.  
1001 East Broadway  
Hawthorne, California  
Attention: Mr. E. Schmued

Ramo-Wooldridge Corporation  
409 East Manchester Blvd.  
Inglewood, California  
Attention: Dr. M. U. Clauser

Ramo-Wooldridge Corporation  
409 East Manchester Blvd.  
Inglewood, California  
Attention: Dr. Louis G. Dunn

The RAND Corporation  
1700 Main Street  
Santa Monica, California  
Attention: Librarian

The RAND Corporation  
1700 Main Street  
Santa Monica, California  
Attention: Dr. C. Gazley

The RAND Corporation  
1700 Main Street  
Santa Monica, California  
Attention: Mr. E. P. Williams

Republic Aviation Corporation  
Conklin Street  
Farmingdale, L. I., New York  
Attention: Dr. W. J. O'Donnell

United Aircraft Corporation  
East Hartford, Connecticut  
Attention: Mr. J. G. Lee

Internal

Mr. Frank Goddard  
Mr. George Goranson (Bldg. 79)  
Dr. John Laufer  
Dr. Peter P. Wegener  
Reports Group  
Jet Propulsion Laboratory  
4800 Oak Grove Drive  
Pasadena 2, California

Dr. W. D. Rannie,  
Goddard Professor  
Jet Propulsion Center  
California Institute of Technology

Dr. Julian D. Cole  
Dr. Donald E. Coles  
Dr. P. A. Lagerstrom  
Prof. Lester Lees  
Dr. H. W. Liepmann  
Dr. Clark B. Millikan  
Dr. Anatol Roshko

Aeronautics Library  
Hypersonic Staff and Research Workers (20)  
Hypersonic Files (3)

Foreign Distribution

via AGARD Distribution Centers